NUMERICAL MODELING OF ICE-STRUCTURE INTERACTION

Quarterly Progress Report No. 2

January 1, 1985 - March 31, 1985

Research Supported By
MINERALS MANAGEMENT SERVICE
United States Department of the Interior

Contract No. 14-12-0001-30219
Duration of Contract: 09/28/1984 - 09/30/1985
Contract Amount: $50,000
COTR: Mr. Charles E. Smith

Prepared By
Prof. S. Shyam Sunder - Principal Investigator
Prof. Jerome J. Connor - Co-Principal Investigator

Department of Civil Engineering
MASSACHUSETTS INSTITUTE OF TECHNOLOGY
Room 1-274
Cambridge, Massachusetts 02139

March 31, 1985

TABLE OF CONTENTS

1. INTRODUCTION

OBJECTIVE OF PROPOSED WORK

The objective of this project is to systematically investigate using numerical models the mechanics of deformation and progressive failure in ice for the purpose of predicting global forces and local pressures on offshore structures proposed for deployment in the Arctic. The focus is on ice sheets interacting with rigid cylindrical indenters. The project involves the following three major areas of study:

1. Development of constitutive models to characterize the mechanical behavior of sea ice.
2. Development of finite element methods of analysis to account for the simultaneous occurrence of viscous (rate dependent) and fracture behavior in ice, and time varying contact between ice and structure.
3. Numerical solution of ice-structure interaction processes for selected ice features and structural configurations to predict global forces and local pressures.

BACKGROUND

As much as 30-40 percent of the U.S. undiscovered hydrocarbon recoverable reserves, comparable in magnitude to those of the Persian Gulf, are estimated to lie in the Arctic. The extraction of these resources in an economical and safe manner poses many technical challenges to offshore engineering. At the root of these problems is the severe environment created by perennial ice features that impart global forces and local pressures on structures which are several times greater than those from waves

in non-Arctic environments. Typically, two levels of ice loading are considered for design purposes. Global ice loads govern the overall structural geometry and dimensions as well as the foundation design, while local ice pressures are likely to dictate wall thicknesses and local framing, and may well govern structural cost.

Most of the emphasis in research has been on predicting global forces. Only during recent years, as the focus changed from overall feasibility to preliminary and detailed design, has the importance of local pressures emerged. It is widely recognized that significant uncertainties exist in the ice load models in use today and that some design loads may be overestimated by an order of magntidue. Research is necessary to quantify the uncertainties in ice loads and to develop improved load prediction models for the safe and economical design of structures.

Uncertainties in existing ice load models arise primarily from five sources:

- Incomplete modeling of the mechanical behavior of ice, including temperature and fracture effects.
- Empiricism in existing theoretical models resulting from the use of approximate analysis mdethods.
- Inadequate modeling of the contact forces at the ice-structure interface.
- Neglecting the effect of scale/size on material strength.
- Not accounting for the finiteness of environmental and other forces driving the ice features.

In order to quantify these uncertainties and to better predict global and local ice loads, numerical models are necessary for computer simulation

of ice-structure interaction processes. In contrast to analytical methods, such models can realistically simulate the interaction accounting for spatial-temporal variability in the mechanical behavior of ice and for multiple modes of failure in ice.

The complexity of sea ice behavior is due mainly to:

- Strong dependence on rate of loading, which is spatially and temporally variable in ice features.
- Simultaneous occurrence of ductile, strain-softening, and brittle modes of deformation.
- Pressure sensitivity leading to different strengths in compression and tension (at moderate-to-high rates of loading) and to melting point depression.
- Material anisotropy leading to strength variation by a factor of three.
- Strong dependence on temperature, varying in first year ice from melting point at the water interface to perhaps -50°F at the air interface.
- Strong dependence on internal structure of ice (grain size, fabric, brine volume, salinity, porosity), which is spatially varying particularly in multi-year ice features.

A key aspect in the development of constitutive models is the need for accurate and consistent experimental data on ice, especially to characterize its behavior relating to tensile loading, cyclic loading, multiaxial loading, nucleation and interaction of cracks, material anisotropy, thermal and structural gradients, and fracture toughness. Currently available data is in many cases sufficient to postulate approximate constitutive models.

Numerical simulations can help to establish the importance of more extensive experimentation in quantifying ice-structure interaction processes.

Finite element methods of analysis for simulating ice-structure interaction processes are affected by the following research concerns:

- Rate dependent material behavior with negligible elastic deformation.
- Initiation and propagation of cracks due to fracture.
- Simultaneous occurrence of rate dependent and fracture behavior.
- Adfreeze bond and friction at ice-structure interface.
- Time-varying contact between ice and stucture and between fractured ice features.
- Strain-softening of ice.

STAFFING

Dr. S. Shyam Sunder, Assistant Professor of Civil Engineering, is Principal Investigator for this project while Dr. Jerome J. Connor, Professor of Civil Engineering, is Co-Principal Investigator. In addition, two full-time graduate Research Assistants are participating in this research: Mr. S-K Ting, a doctoral student with considerable experience in concrete testing and dynamic behavior of offshore structures; and Mr. F.S. Chehayeb, a doctoral student whose background is in numerical analysis and finite element methods.

2. SUMMARY OF RESEARCH ACTIVITIES

The principal technical developments through the end of this reporting period have been:

(1) The study of sea ice indentation in the creeping mode of deformation.

(2) Initiation of research to develop failure criteria for sea ice accounting for fracture behavior.

Specific accomplishments and current research directions are discussed below:

Sea Ice Indentation in the Creeping Mode

A study of ice indentation in the creeping mode is important for two reasons: (a) creep is the predominant mode of deformation for artificial islands in the Arctic nearshore region during "breakout" and/or steady indentation conditions occurring in the winter, and (b) stresses, strains, and strainrates within the continuum resulting from creep are necessary to predict the initiation and possibly even the propagation of cracks when viscous effects influence fracture.

Global and local pressures generated during sea ice indentation in the creeping mode are being studied, accounting for the spatial variation of strainrates. Two methods of analysis are being considered: (a) approximate methods, i.e., upper-bound method and strain path method, and (b) "exact" method based on the finite element method. In both cases, a two-dimensional idealization of the indentation process is considered. In order to provide continuity with previous work, the isotropic, incompressible three-dimensional extension of the uniaxial power-law creep model has been extensively studied. Pressures predicted with this model are

being compared with those from previously published formulas, e.g., API Bul. 2N, Ponter et al., and Bruen & Vivatrat. In addition, ice pressures have been obtained with the approximate methods for a new uniaxial model that accounts for the stress-strain-strainrate behavior of sea ice, including its strain-softening behavior.

The key difference in the two approximate methods of analysis is that point stresses within the continuum can be obtained with the strain path method. As a result, local stresses at the ice-structure interface can be estimated, unlike the upper bound method which only yields the global pressure. However, both methods rely on an adequate specificiation of the velocity field in the ice sheet. This is obtained through a combination of theoretical modeling based on fluid mechanics and field ice movement survey data from an artificial island in the Beaufort Sea. In particular, two theoretical kinematic models are considered: one resulting from the superposition of a point source and a uniform flow (Kinematic Model A) that has been proposed by Bruen & Vivatrat; and the other resulting from the superposition of a doublet and a uniform flow (Kinematic Model B).

The results of the approximate methods indicate that:

(a) Kinematic Model B better models the ice movement survey data used here than Kinematic Model A.

(b) In the creeping mode of ice deformation, local ice pressures are of the same order of magnitude as the global pressures.

(c) Under the same conditions, Kinematic Model B, the API model, and the Ponter et al. model predict similar global pressures.

(d) The variation in global pressures for different power-law model parameters (Wang, Sanderson, Ting & Shyam Sunder) is on the order of 30%.

A key finding of the work is that for rate-dependent material models describing sea ice behavior, interface adfreeze and friction stresses can significantly influence both local and global ice pressures. The only realistic way to study these effects is through numerical models based on the finite element method of analysis.

This research has been summarized in a paper entitled "Sea Ice Indentation Accounting for Strain-Rate Variation" to be published in the proceedings of the ASCE Specialty Conference: ARCTIC '85 - Civil Engineering in the Arctic Offshore to be held at San Francisco, CA, March 25-27, 1985. A copy of the paper is attached in Appendix A.

The finite element formulation for general viscoplastic behavior including creep (nonlinear viscoelasticity) has been implemented in a computer code called DECNEC (Discrete Element Computational NEtwork Controller). A major effort has been expended in developing a new bi-level solution algorithm. This is based on a secant type iteration involving 4-6 cycles per time step on the global equations of motion and a Newton-Raphson or tanget type iteration, combined with the α-method of time integration and typically not exceeding 4 cycles per time step, on the rate-dependent constitutive relations at each integration point within an element. Data input is simplified by the use of a pre-processor specially written for the program. A post-processor called ORION, originally developed at the Lawrence Livermore Laboratory, can produce graphical display of stress, strain, and strainrate contours as well as interface pressure distributions. The current implementation is a two-dimensional version for plane stress problems. A four noded quadrilateral element is currently available. Although an eight-noded quadratic element is often preferred (and may be

included in the future), accurate results can and have been obtained with the four-noded element using a finer finite element mesh. The program has the ability to simulate a free or frictional contact between two deformable bodies, i.e., no contact stresses due to adfreeze bond, by defining the interface as a "slideline". An isotropic power-law creep material model has been implemented in the present version of the program.

The accuracy of the computer code has been verified in two ways; through the solution of simple test problems, and by comparing the variability in predicted global pressures due to indenter diameter, material model parameters, and ice sheet velocity with that predicted by approximate methods of analysis. In both cases, the numerical solutions are accurate to within specified tolerances typically achievable in finite element analyses.

Numerical simulations have been performed under plane stress conditions to assess the influence of interface adfreeze and friction, material constants for a multi-axial power law creep model, grounded rubble pile, and ice sheet velocity on predicted global forces and local pressures. The results have been compared with those based on approximate methods of analysis. Stress, strainrate, and strain countours have been obtained in addition to the distribution of interface pressures.

The numerical simulations show that:

1. Global forces vary by a factor of 2.5 depending upon whether the interface condition is fixed (infinite adfreeze bond strength), roller, or free (no adfreeze bond strength or interface friction). The fixed condition is about 1.3 times and the free condition about 0.5 times the roller condition.

2. Finite element analysis predictions of global pressure differ from a modified form of the upper bound solution for Kinematic Model B by less than 10% for varying velocity, indenter diameter, and material constants. The modification is necessary since the two-dimensional nature of the kinematic models makes the approximate solutions strictly apply to plane strain conditions, and not to the plane stress condition of interest.
3. The ratio of maximum normal interface pressure to global pressure approximately varies in the range 0.35-1.10 depending upon the interface condition. It is 0.35 for the fixed condition, 0.55 for the roller condition, and 1.10 for the free condition.
4. The maximum (peak) normal interface pressures vary by a factor of 1.26 depending upon the interface condition. The fixed condition is about 0.83 times and the free condition about 1.04 times the roller condition. The maximum interface shear stress for the fixed condition is about 0.81 times the corresponding maximum normal pressure. However, a different boundary value problem involving a smaller contact area, as opposed to contact over half the perimeter in the free condition, will lead to higher interface pressures.
5. Pressure-area curves should be considered as providing the maximum normal interface pressure for a given indenter area of contact (form area), rather than the average integrated normal pressure over a tributary loaded area for a structural component. It is conservative to assume a uniform or rectangular distribution of the local pressure over the indenter area of contact for purposes of design.

6. Tensile stresses, strains and strainrates occur almost all over the ice sheet, and may be the key to explaining fracture behavior during indentation. While biaxial compression and tension states tend to occur for stress on the upstream and downstream sides, respectively, the state of strain is almost always compression-tension. The levels of tensile strain are often sufficient to cause cracking even before steady state creep is reached.

The possible effect of a grounded rubble pile or accreted ice foot on ice pressures was assessed by defining an effective indenter equal to a multiple (2.85) of the structural diameter. This resulted in a factor of 1.97 increase in global force. In the case of a grounded rubble pile, it would be over conservative to consider that all this force is transmitted to the foundation by the structure. On the other hand, the force transmitted to the foundation by the structure would decrease by a factor of 4.14 if both the structure and the grounded rubble pile could transmit a force proportional to the contact area of each with the foundation. This may be reasonable only if the rubble pile is consolidated and grounded fimly in the foundation soil such as in the case of constructed ice packs. Further research is necessary to quantify the level of force that can be directly transmitted to the foundation by a grounded rubble pile.

The numerical simulations also showed that (i) even a factor of two uncertainty in velocity will affect ice pressures only by about 20-30%, and (ii) uncertainties in material constants for an isotropic power law creep model may yield ice pressures that vary by about 15-30%. However, improved material models that include fracture and temperature effects in addition to the transversely isotropic behavior of sheet ice can have a major influence

on ice pressure predictions. In particular, fracture in ice will be the key mechanism that limits ice pressures generated under the significantly higher velocities that occur in the field when compared with the value just prior to "breakout" or macrocracking considered here. This is an area for further research.

This research has been summarized in a paper entitled "Sea Ice Indentation in the Creeping Mode" to be published in the proceedings of the 17th Annual Offshore Technology Conference, Houston, TX, May 6-9, 1985. A copy of the paper is attached in Appendix B.

Failure Criteria for Sea Ice

Field observations of sea ice identation on offshore structures in the Arctic show that fracture processes are a major factor in ice-structure interaction.

Fracture manifests itself in terms of tensile cracking and crushing in compression. Numerical simulations of ice-structure interaction processes in the creeping mode of deformation have indicated that the ice sheet consists of three regimes of principal stresses and strains; i.e., compression-compression, compression-tension, and tension-tension. The latter two regimes occupy a major fraction of the area of the continuum. Since ice is weaker in tension than in compression once cracks occur, accounting for the differing behavior of ice in tension may help to reduce (or limit) ice force predictions significantly.

The uniaxial stress-strain-strainrate material model developed for ductile and strain-softening modes of deformation in sea ice has been extended to account for compression fracture and tensile cracking. The

adequacy of the model has been demonstrated by comparison with experimental data obtained under constant strainrate, creep, and constant stressrate conditions. The model has been used to predict the occurrence of first cracks in ice under uniaxial compressive loading. Tensile strains occur under this loading condition as a result of the Poisson effect and/or incompressibility condition. Once cracks occur, the material continues to sustain compressive load but loses its ability to carry tensile loads in the transverse direction if applied. This is a realistic assumption and has been used often in modeling concrete behavior. A limiting tensile strain criterion dependent on the instantaneous strainrate in tension has been used to predict crack nucleation. The results for compressive creep compare very well with the experimental data of Gold.

This research has been summarized in a paper entitled "Ductile to Brittle Transition in Sea Ice Under Uniaxial Loading" to be published in the proceedings of the 8th International Conference on Port and Ocean Engineering under Arctic Conditions, Greenland, September 7-14, 1985. A copy of the paper is attached in Appendix C.

3. RESEARCH OBJECTIVES AND PLANS FOR NEXT YEAR

The proposed research area is broad and complex. A systematic approach is being followed to address the overall research objectives during the course of the current research project which spans a three-year term commencing September 1984. The following discussion identifies specific topics that will be receiving major attention in the next 12-18 months.

1. A study of sea ice indentation in the creeping mode using a finite element method of analysis to quantify the effect of material anisotropy on ice loads: First-year columnar sea ice displays strong material anisotropy in a direction perpendicular to the plane of the ice sheet. Experiments have shown that the ratio of vertical to horizontal strength in the ice sheet lies in the range 2-5 for a wide range of strain rates. Plasticity type solutions based on approximate methods of analysis have shown this to have significant influence on global ice forces. The objectives of the research are to postulate a multiaxial power law creep model accounting for material anisotropy (assuming transverse isotropy), to calibrate it with available data, and to implement the model in the finite element analysis computer code DECNEC. A major effort will be required to modify the current solution algorithm to incorporate this new material model. The effect of material anisotropy on both global forcces and local pressures will then be quantified through numerical simulations. The results will be calibrated with those from approximate methods of analysis.

2. Development of a multiaxial constitutive model: A new constitutive model for sea ice, applicable to monotonic uniaxial loading in both compression and tension, has been proposed and calibrated with experimental

data. The stress-strain-strainrate behavior of sea ice has been modelled accounting for strain softening and for fracture which manifests itself in terms of tensile cracking and crushing in compression. The model has been used to predict first cracking in ice under uniaxial compressive loading based on a limiting tensile strain criterion and the results have been calibrated with experimental data available in the literature. However, prior to implementing the model within a finite element analysis framework to predict ice forces and pressures, it is necessary to extend the model to account for unloading/reloading and multiaxial effects. This will be the focus of a major research effort during the next several months. Among the approaches that will be investigated to develop a general and unified constitutive model that captures the important features of ice behavior are the plastic-fracturing theory and the endochronic theory, both of which have been extensively investigated in recent years for somewhat similar applications in concrete. The model will be calibrated with experimental data for first year sea ice being generated at CRREL. The initial emphasis will be on obtaining a constitutive model adequate to characterize sea ice indentation under plane stress conditions.

3. A study of sea ice indentation accounting for rate dependent and fracture behavior using a finite element method of analysis: The quantification of fracture behavior requires two criteria, one for initiation and the other for propagation. Fracture initiation can often be well described by a strain criterion. However, two alternative approaches are available to describe fracture propagation: a tensile limiting strain or strength criterion, and a fracture mechanics criterion based on a pre-existing distribution of cracks in the continuum. The former approach for fracture

propagation can be used to model fracture behavior in a material originally in virgin (flawless) form.

In the case of load bearing systems such as structures, a fracture mechanics criterion for cracking is conservative. However, in the case of load transmitting systems such as ice features, a fracture mechanics approach may lead to unconservative results. In order to account for tensile cracking and compressive fracture in ice and still be conservative in force and pressure predictions, a limiting strain or strength criterion is preferable to the fracture mechanics approach. It is the former criterion that we will be adopting for this project.

Several approaches are available to account for cracking in a finite element framework. Two of the more common approaches are the discrete cracking models which follow individual discrete cracks between elements and the smeared cracking models which treat the gross (smeared) effect of cracks in an element. The latter approach has been preferred in finite element analyses of concrete since it is computationally far more convenient, and will be adopted in this project.

Smeared crack models have one apparent disadvantage; the results are sensitive to the size of the finite elements in the mesh. For ice-structure interaction in the presence of flaws, the coarser the mesh the more conservative will the load prediction be. For fraction initiation and propagation in an initially flawless material (assumed here), the size problem can be completely avoided, at least theoretically, if the element size is identical to the size of the ice specimen for which the constitutive model applies. A coarser mesh will lead to conservative results. The degree of conservatism can be assessed by progressively refining the mesh.

A major research effort is being undertaken to (1) extend the plane stress finite element analysis computer code to incorporate smeared cracking models, and (2) implement the constitutive model in the program. The influence of fracture on both global forces and local pressure will then be quantified through numerical simulations.

4. NOTABLE NON-TECHNICAL ACTIVITIES

PUBLISHED OR SUBMITTED PAPERS

1. Ting, S-K., and Shyam Sunder,, S., "Sea Ice Indentation Accounting for Strain-Rate Variation," Proceedings of the ASCE Speciality Conference: ARCTIC '85 - Civil Engineering in the Arctic Offshore, San Francisco, CA, March 25-27, 1985.

2. Chehayeb, F.S., Ting, S-K., Shyam Sunder, S., and Connor, J.J., "Sea Ice Indentation in the Creeping Mode," Proceedings of the 17th Annual Offshore Technology Conference, Houston, TX, May 6-9, 1985. Paper to be simultaneously reviewed for publication in the Journal of Engineering Mechanics, ASCE.

3. Shyam Sunder, S., and Ting, S-K., "Ductile to Brittle Transition in Sea Ice Under Uniaxial Loading," Proceedings of the 8th International Conference on Port and Ocean Engineering Under Arctic Conditions, Narssarssuaq, Greenland, September 6-13, 1985. Expanded version of paper to be submitted for publication in Cold Regions Science and Technology.

SEMINARS AND TALKS

1. Both Professors S. Shyam Sunder and Jerome J. Connor participated in the Workshop on Breaking Process of Ice Plates held at M.I.T. on November 1-2, 1984. The title of their presentations are listed below:

   a. Professor S. Shyam Sunder: Sea Ice Indentation Accounting for Strain-Rate Variation.

   b. Professor Jerome J. Connor: Numerical Simulation of the Creep Mode in Ice-Structure Interaction.

   Professor S. Shyam Sunder was invited to talk on the same topic at the weekly seminar of the Constructed Facilities Division of the Department of Civil Engineering at MIT on December 5, 1984.

2. Professor S. Shyam Sunder was invited to talk on "Sea Ice and Its Mechanical Behavior" at a series of seminars on Engineering in the Arctic organized during MIT's Independent Activities Period, January 1985.

PROFESSIONAL ACTIVITIES

1. Professor S. Shyam Sunder is a member of the Conference Committee for ARCTIC '85 - Civil Engineering in the Arctic Offshore Speciality Conference of the ASCE to be held in San Francisco, March 25-27, 1985. He is also moderating a session on Probabilistic Methods in Arctic Offshore Engineering.
2. Professor S. Shyam Sunder has been appointed Chairman of ASCE's Subcommittee on Arctic and Frontier Regions. This subcommittee operates under the ASCE Structural Division's Committee on Reliability of Offshore Structures.
3. Professor S. Shyam Sunder is a member of the ASCE TASK Committee on Reliability-Based Techniques for Designing Offshore Arctic Structures which is entrusted with the responsibility of producing a monograph bearing the same name.
4. Professor S. Shyam Sunder attended the Arctic Energy Technologies Workshop organized by the U.S. Department of Energy as part of a recently initiated Arctic and Offshore Research Program. The workshop was held at Morgantown, West Virginia, on November 14-15, 1984. He also participated in the discussion group on Arctic Offshore Structures which had the task of defining the state-of-the-art, identifying technical issues, listing research and development needs, and recommending topics for research support by the U.S. DOE.
5. Professor S. Shyam Sunder participated in a workshop on "Northern Research Needs in Civil Engineering" organized by the University of Alaska, Fairbanks, in Seattle, WA, February 16-17, 1985. The workshop was sponsored by the National Science Foundation to help formulate a five

year plan for Arctic research under its mandate for implementing the Arctic Research & Policy Act of 1984. Professor Shyam Sunder contributed to the Committee on Offshore and Coastal Facilities, Design and Construction.

6. Professor Jerome J. Connor is leading the organization of an International Conference on Ice Technology (ITC '96) to be held at MIT, June 10-12, 1986. An international Scientific Advisory Committee has been set up with Professor Connor and Dr. C.A. Brebbia of Southampton University, England, as Co-Chairmen. This conference will be sponsored by the Center for Scientific Excellence in Offshore Engineering at MIT, the Centre for Advanced Engineering Studies at the University of Southampton, and the MIT Sea Grant Program. Announcement and Preliminary Invitation to the conference is expected to be mailed shortly.

EXPERIMENTAL DATA FROM U.S. ARMY CRREL

An informal agreement has been reached with the U.S. Army Cold Regions Research and Engineering Laboratory, Hanover, N.H., Group under the leadership of Dr. Gordon Cox concerning our use of experimental data obtained by them. Under this agreement we can have immediate access to all their experimental data, although any publication by us of their data would in general be dated after they have had an opportunity to publish the results themselves.

5. BUDGET

The total expenditure as of February 28, 1985 is $20,886.39. This reflects expenditures for the six month period September 1, 1984 (the requested project starting date) through the end of February.

Professor S. Shyam Sunder charged 10% of his salary to the project and 20% to the SOHIO account through January 31, 1985. From February 1, 1985 he is charging 20% of his salary to the MMS account, and an equal amount to the SOHIO account. Professor Jerome J. Connor is charging 10% of his salary to the MMS account and 10% to the SOHIO account. This is expected to remain unchanged through May 31, 1985, i.e., the academic year.

Mr. S-K Ting and Mr. F.S. Chehayeb are full-time Research Assistants on the project. During the Fall Term their salary was charged to the SOHIO account. During the Spring Term their salary is being charged to the MMS account.

SEA ICE INDENTATION ACCOUNTING FOR STRAIN-RATE VARIATION

Seng-Kiong Ting[1] and S. Shyam Sunder[2], A.M., A.S.C.E.

November 1, 1984

To be presented at the
A.S.C.E. Specialty Conference
ARCTIC '85 - Civil Engineering in the Arctic Offshore
San Francisco, CA
March 25-27, 1985

[1]Research Assistant, Department of Civil Engineering, Massachusetts Institute of Technology, Room 1-225, Cambridge, MA 02139.

[2]Assistant Professor of Civil Engineering, Massachusetts Institute of Technology, Room 1-274, Cambridge, MA 02139 (Tel. 617-253-7118).

SEA ICE INDENTATION ACCOUNTING FOR STRAIN-RATE VARIATION

Seng-Kiong Ting[1] and S. Shyam Sunder[2], A.M., A.S.C.E.

ABSTRACT: Global and local indentation pressures in the creeping mode of sea ice deformation are obtained, accounting for the spatial variation of strain-rates. Two approximate methods of analysis are considered; the upper bound and strain path methods. Theoretically postulated velocity fields required in the analysis are calibrated with field measurements. Sea ice behavior is described by a multi-axial power-law creep model and by the multi-axial extension of a new uniaxial model which accounts for both hardening and softening behavior. Results are compared with previously published indentation formulas.

INTRODUCTION

Two levels of ice loading are typically considered in the design of drilling and production platforms for the Arctic. Global ice pressures govern the overall structural geometry and dimensions as well as the foundation design, while local pressures are likely to dictate wall thicknesses and local framing, and may well govern structural cost. Most of the emphasis on ice force research has been on predicting global forces. Only during recent years, as the focus changed from overall feasibility to preliminary and detailed design, has the importance of local pressures emerged. Peak local pressures may be as high as three times the average global pressure. It is widely recognized that uncertainties exist in ice load prediction models in use today and that in some cases design loads may be overestimated by an order of magnitude.

Uncertainties in existing ice load models arise primarily from four sources: (i) incomplete modeling of the thermomechanical behavior of sea ice, (ii) use of semi-empirical formulations, calibrated without adequate regard for similitude modeling and scale effects, (iii) failure to realistically model the contact forces at the ice-structure interface and the presence of macrocracks, and (iv) not accounting for the finiteness of the environmental forces driving the ice features. Both approximate analytical methods and more rigorous numerical models based on the finite and boundary element methods of analysis can be used to study ice-structure interaction at full scale with realistic models for material and interface behavior.

This paper employs two approximate methods of analysis, the upper bound and strain path methods, to study the problem of sea ice indentation in the creeping mode of deformation, accounting for the spatial variation of strain-rates. This is a problem of concern for artificial islands in the Arctic nearshore region, where "break-out" and/or steady indentation conditions occurring in the winter form a basis for select-

[1]Research Assistant, Department of Civil Engineering, Massachusetts Institute of Technology, Cambridge, MA 02139

[2]Assistant Professor of Civil Engineering, Massachusetts Institute of Technology, Room 1-274, Cambridge, MA 02139

ing design ice loads. The key difference in the two analyses is that point stresses within the continuum can be obtained with the strain path method. As a result, local stresses at the ice-structure interface can be estimated, unlike the upper bound method which only yields the global pressure. However, both methods rely on an adequate specification of the velocity field in the ice sheet. This is obtained through a combination of theoretical modeling based on fluid mechanics and field ice movement survey data from an artificial island in the Beaufort Sea. In particular, two theoretical kinematic models are considered: one resulting from the superposition of a point source and a uniform flow (Kinematic Model A) that has been studied previously (3,9); and the other from the superposition of a doublet and a uniform flow (Kinematic Model B).

An important aspect of the analysis is the specification of the mechanical behavior of sea ice. In order to provide continuity with previous work, the isotropic, incompressible three-dimensional extension of the uniaxial power-law creep model is studied. The predicted global ice pressures are compared with those from previously published formulas (1,8). Finally, a new uniaxial law that models the stress-strain-strainrate behavior of sea ice, including its strain-softening behavior, is presented. The strength-strainrate relationship derived from this new model is used to predict global ice pressures during indentation.

BOUND METHOD VERSUS STRAIN PATH METHOD

An upper bound (conservative) solution to a continuum mechanics problem may be derived by relaxing the statical field equations and boundary conditions, and using velocity fields that satisfy the kinematic constraints for the problem. Applying the principle of virtual work and Drucker's convexity criterion, the upper bound estimate of the global load for incompressible materials may be obtained with (4):

$$\int_V S^*_{ij}\,\dot{\varepsilon}^*_{ij}\,dV \geq \int_{S_T} T_i U^*_i\,dS + \int_{S_U} T_i U_i\,dS \qquad (1)$$

where S^*_{ij}, $\dot{\varepsilon}^*_{ij}$ and U^*_i are the deviatoric stresses, strain-rates and velocities obtained from an assumed kinematically admissible velocity field. T_i and U_i are the actual surface tractions and velocities.

The upper bound method does not make use of the field equilibrium equations. As such, point stresses in the continuum are unknown. Hill (5) has suggested an approximate method by which octahedral (hydrostatic) stresses can be derived from deviatoric stress gradients using the equilibrium equation. This idea was developed and first applied to deep penetration problems in soil mechanics by Baligh (2), who called it the strain path method.

In applying the strain path method to the ice indentation problem, the major assumption is that the strain and strain-rate field can be obtained from the kinematic conditions with no reference to constitutive relations, equilibrium equations, or statical boundary conditions. This is an approximation and hence the derived stress field is approximate in general. However, the method is computationally very attractive when compared with a detailed finite element analysis. In addition, the method provides valuable insights to the indentation problem which is difficult to obtain from a purely numerical approach.

KINEMATIC MODELING OF ICE SHEET

Theoretical Kinematic Models.-- Kinematic Model A is shown in Fig. 1. The streamline passing through the stagnation point defines the bluff-body, i.e., the region where the oncoming sheet of ice cannot enter. The streamfunction, ψ, and flow velocities, U_r and U_θ, follow from the theory of fluid mechanics and are given by:

$$\psi = - U_o r \sin \theta - U_o a \theta \tag{2}$$

$$U_r = \frac{-1}{r} \frac{\partial \psi}{\partial \theta} = U_o \cos \theta + U_o \frac{a}{r} \tag{3}$$

$$U_\theta = \frac{\partial \psi}{\partial r} = - U_o \sin \theta \tag{4}$$

where U_o is the uniform far field velocity. The bluff-body is described by $r=a(\pi-\theta)/\sin \theta$ with the half-width of the body at $r=\infty$ equal to πa. This model assumes that the normal velocity at the ice/bluff-body interface is zero. Even if this is valid, the tangential contact between the moving ice sheet and the half-body could in general be either friction-free or possess finite frictional forces. This imposes a statical boundary condition with which the chosen velocity field may or may not be consistent.

Kinematic Model B is shown in Fig. 2. The bluff-body in this case is a circle of radius, a. This represents flow past a cylindrical indenter with contact at all points on the circumference. The streamfunction and flow velocities are given by:

$$\psi = - U_o r \sin \theta + U_o \frac{a^2}{r} \sin \theta \tag{5}$$

$$U_r = U_o \left[1 - \frac{a^2}{r^2}\right] \cos \theta \tag{6}$$

$$U_\theta = - U_o \left[1 + \frac{a^2}{r^2}\right] \sin \theta \tag{7}$$

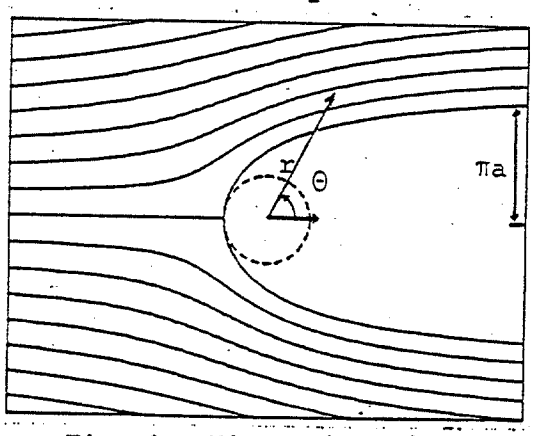

Fig. 1.--Kinematic Model A

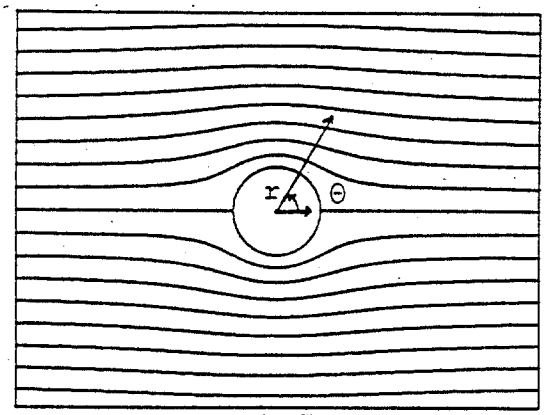

Fig. 2.--Kinematic Model B

Calibration with Field Ice Movement Data.-- The theoretical velocity fields are calibrated with field ice movement data from an artifical island in the Beaufort Sea, obtained over a period of seven weeks during peak winter ice formation. The surveys were carried out at the 39 stations at least once per day, although during high movement events the

surveys were made every 12 hours. The calibration is based on the following three criteria: (a) streamfunction values for a particle at the start and end of the observation period should be equal under steady flow conditions; (b) the average movement rate measured should be approximately equal to the average of the predicted velocities over the observation period; and (c) the measured direction of movement must equal the predicted bearing.

A careful analysis of the data shows that the ice movements downstream and directly at the back of the indenter are of the same order of magnitude as on the upstream side prior to macrocracking, which was observed to occur in a direction perpendicular to the flow on the downstream side. Thus Kinematic Model A which considers no flow within the bluff-body cannot model field conditions prior to macrocracking. Nevertheless, both kinematic models predict relatively accurate streamfunction values over their respective domains of applicability. For Model A the errors vary from less than 1% to as much as 25%, even when there is no macrocrack formation. For Model B, the errors are generally less than 1% in all cases except the case with macrocrack formation. The errors in velocity predictions are much higher for both models. Some stations near the rubble pile surrounding the structure are significantly in error due to an inadequate modeling of the structural geometry, e.g., choice of diameter D. In the cases affected by macrocracking: (a) separate and large regions of the continuum are adequately modeled by both velocity fields, (b) Model B is in general better than Model A. Typical errors in the velocity are on the order of 5% to 10% if the above exceptions are taken into account. The errors in bearing predictions are on the order of 5 to 10 degrees for Kinematic Model B and larger for Model A. The discrepancies, where they are larger, can be explained with arguments similar to that for velocities.

In summary: (a) Kinematic Model A does not adequately model the field data considered here; (b) Kinematic Model B provides a good description of the measured flow field and can be used to explain the observed macrocracking if tensile stresses develop on the downstream side; (c) even after macrocracking, Model B accurately models the upstream flow field; and (d) the transition from creeping behavior to macrocracking occurs for velocities less than 1 ft/hr (85×10^{-6} m s^{-1}).

ICE PRESSURES FOR POWER-LAW CREEP MODEL

The isotropic, incompressible three-dimensional extension of the uniaxial power-law creep leads to the following constitutive model:

$$S_{ij} = \frac{2}{3} \left(\frac{\sigma_o}{\dot{\varepsilon}_o} \right)^N \dot{\varepsilon}_e^{\frac{1}{N} - 1} \dot{\varepsilon}_{ij} \qquad (8)$$

where S_{ij} and $\dot{\varepsilon}_{ij}$ are the deviatoric stress and strain-rate tensors, respectively. The effective strain-rate is defined as:

$$\dot{\varepsilon}_e = \left[\frac{2}{3} \dot{\varepsilon}_{ij} \dot{\varepsilon}_{ij} \right]^{1/2} \qquad (9)$$

N is the power-law exponent; σ_o and $\dot{\varepsilon}_o$ are material constants derivable from uniaxial testing of ice. The results presented in this paper are based on the sea ice data of Wang (10).

The basic steps for evaluating stresses using the strain path method are: (a) compute the strain-rate field by differentiating the veloci-

ties with respect to the spatial coordinates, (b) evaluate the deviatoric stress field using the constitutive equations, (c) obtain octahedral stresses by spatially integrating the equilibrium equations (the octahedral stresses will in general be path dependent), and (d) estimate the total stresses by summing the deviatoric and octahedral stresses. Then, the local stresses at the ice-structure interface can be obtained from the total stress field, while global pressures may be estimated with the bound method and/or by integration of the local stress field.

The degree of approximation in the estimated stress field can be assessed by comparing the octahedral stresses obtained by integration along different (i.e., orthogonal) paths and by noting the error in satisfying statical boundary conditions. Another way of making the former comparison is to integrate along one path and to compare the magnitude of fictitous body forces required for equilibrium in the orthogonal direction with the stress gradients in that direction.

Ice Pressure Prediction.-- Results from the application of the upper bound and strain path methods of analysis to the chosen kinematic models are presented below.

1. Kinematic Model A: The octahedral stress field for this kinematic model is path independent and as such equilibrium is exactly satisfied. In spite of this, the statical interface boundary conditions may not be satisfied by the model. In addition, the following comments can be made:

(i) the maximum strain-rate occurs at the ice/bluff-body interface at r=a, and is equal to U_o/a,
(ii) the stress field decays as $r^{-2/N}$, which for N=4 is $1/\sqrt{r}$,
(iii) the stress field is axisymmetric, and
(iv) the octahedral stress is zero for a viscoelastic material (N=1).

The global pressure can be estimated by the upper bound method, assuming a frictionless ice/bluff-body interface. This is similar to the case studied by Bruen and Vivatrat (3), and Eq. (1) reduces to:

$$\frac{P}{2at} \leq \frac{N}{\sqrt{3}} \int_0^{\pi} \left(\frac{\sin\theta}{\theta}\right)^{2/N} d\theta \left[\frac{2}{\sqrt{3}} \frac{\sigma_o^N}{\dot{\varepsilon}_o} \frac{U_o}{a}\right]^{\frac{1}{N}} \qquad (9)$$

A second approach to estimating the global pressure involves integration of the local stresses around the bluff-body, i.e.,

$$P = t \int (\sigma_{rr} \cos\theta \, r d\theta + \sigma_{\theta\theta} \sin\theta \, dr) \qquad (10)$$

Using the equation for the bluff-body, Eq. (10) shows that P=0, unlike the upper bound method. If the frictional forces predicted by the strain path method at the ice/bluff-body interface are included in the upper bound method, that method also predicts zero pressure. However, the bound theorems do not apply for the case of friction with relative motion. The implications of this finding are more fully discussed for Kinematic Model B.

2. Kinematic Model B: The octahedral stresses for this kinematic model are path dependent, although for N=1 and N=3 the fictitious body force is zero and equilibrium is satisfied exactly. However, the statical interface boundary conditions will in general not be satisfied. In addition, the following comments can be made:

(i) the maximum strain-rate occurs at the ice-structure interface, r=a, and is equal to $2U_o/a$ or $4U_o/D$,

(ii) the stress field decays as $r^{-3/N}$ (not $r^{-2/N}$ as predicted by Kinematic Model A), which for N=4 is $r^{-3/4}$,

(iii) the stress field is not axisymmetric, and

(iv) the octahedral stress is zero for a viscoelastic material.

The radial stresses downstream of the indenter are tensile and equal in magnitude to the upstream compressive stresses, consistent with the material law. The tangential stresses behave similarly for typical values of N, although their magnitudes could be less than half of the radial stresses. These are principal stresses at $\theta=0$. As such, it is reasonable to expect a macrocrack formation on the downstream side of the indenter. This is indeed borne out by the field ice movement data.

The global pressure can be estimated using the bound method, assuming either a frictionless interface or an interface with frictional stresses predicted by the strain path method. (The method does not strictly apply for the latter case.) The respective expressions, derived from Eq. (1) for D=2a, are:

No friction

$$\frac{P}{Dt} \leq \frac{4\pi}{\sqrt{3}} \frac{N}{N+3} \left[\frac{4}{\sqrt{3}} \frac{\sigma_o^N}{\dot{\varepsilon}_o} \frac{2U_o}{D} \right]^{\frac{1}{N}} \qquad (11)$$

With friction

$$\frac{P}{Dt} \leq \sqrt{3}\pi \frac{N-1}{N+3} \left[\frac{4}{3} \frac{\sigma_o^N}{\dot{\varepsilon}_o} \frac{2U_o}{D} \right]^{\frac{1}{N}} \qquad (12)$$

The ratio of Eq. (11) to Eq. (12) is $4N/3(N-1)$, which varies between 1.8 and 2.2 for $2.5 \leq N \leq 4$. Intuitively, interface friction should increase indentation pressures. However, both kinematic models studied here predict a significant decrease in pressure. This is because they are derived from considerations for ideal, non-viscous fluids and as such do not correctly model interface conditions. Even if more exact velocity fields can be postulated theoretically, the available field data does not provide adequate resolution of the ice movements in the immediate vicinity of the structure to calibrate the kinematic models.

Integration of the local stresses around the bluff-body yields another estimate of global pressure accounting for the frictional stresses of the strain path method:

$$\frac{P}{Dt} = \frac{\pi}{2\sqrt{3}} (N-1) \left[\frac{4}{\sqrt{3}} \frac{\sigma_o^N}{\dot{\varepsilon}_o} \frac{2U_o}{D} \right]^{\frac{1}{N}} \qquad (13)$$

Both Eqs. (12) and (13) predict zero pressure for a viscoelastic material. Furthermore, the ratio of the upper bound method to Eq. (13) is $6/(N+3)$, which varies between 0.86 and 1.09 for $2.5 \leq N \leq 4$.

For the artificial island considered in this paper the maximum strain-rate just prior to macrocracking is on the order of 10^{-6} s^{-1} or less. The peak local tangential stresses are on the order of 80 psi (0.55 MPa), the peak local radial stresses are on the order of 320 psi (2.2 MPa). The radial stresses are compressive upstream of the indenter and tensile on the downstream side, and are distributed in a cosinusoidal fashion. The typical order of magnitude value for the global pressure obtained with Eq. (13) is about 350 psi (2.4 MPa). A key inference here is that the local and global pressures are on the same order of magnitude. If instead Eq. (11) is used to estimate the global pressure, the peak local pressure becomes approximately half the global pressure.

Table 1.--Comparison of Average Global Pressures for Power-Law Creep with N=4 and Average Strain-Rate of $U_o/2D$

Model	Constraints	ϕ
API	Plane Strain	4.12
	Plane Stress	3.13
Ponter et al. (1983)	Plane Strain	3.64
	Plane Stress	1.85
Model A	$D = 2\pi a$	3.22
	$D = 2a$	7.60
Model B		7.22

Comparison with Other Ice Pressure Formulas.-- Average global pressures during sea ice indentation can be estimated using any one of the many predictive models available in the literature. In this study, the global pressures predicted by Kinematic Models A and B, neglecting interface frictional stresses, are compared with the models of API (1) and Ponter et al. (8). The general form of all these models is given by:

$$\frac{P}{Dt} = \phi\ \sigma(\dot{\varepsilon}_a) \qquad (14)$$

where ϕ is a constant depending in general on N, and $\sigma(\dot{\varepsilon}_a)$ is the uniaxial strength of ice evaluated at some average strain-rate, $\dot{\varepsilon}_a = U_o/(\phi\Psi D)$ with Ψ being a second constant. In order to compare the various formulations, $\phi\Psi$ is assumed equal to two as suggested by API (1) and the comparison can therefore be based on the parameter ϕ.

The values of ϕ predicted by the four formulations for a power-law creep model with N=4 is given in Table 1. At first glance the numbers seem highly scattered, varying from 1.85 to 7.60. However, there are important differences among the models. The first two formulations apply for a flat indenter with ice pressures being allowed to develop only on the upstream side. For the API model, the sea ice is assumed columnar and the contact factor is set to one. In Ponter et al.'s model, a correction factor of 1.1 is applied to ϕ to make results consistent with N=4. In Kinematic Model A, the problem geometry (Fig. 1) is different from the other models and the choice of indenter diameter is subjective. If the indenter diameter is chosen as $2\pi a$, ϕ is about 42% of that for D=2a. In the former case the indenter is located far away ($r \to \infty$) from the tip of the bluff-body with the region in between consisting of inert ice, while in the latter case the indenter is located at the tip of the bluff-body with the inert region downstream of the indenter. Field data on deformation patterns considered here indicate that both assumptions may be unrealistic. The ϕ factor for Model B is based on a circular indenter with compressive and tensile stresses on the upstream and downstream sides respectively. This is more representative of actual field conditions prior to breakout.

If the API and Ponter et al. models are extended to account for downstream tensile stresses, the ϕ factors would probably be twice as much since for the problem and material model considered (a) tensile and compressive strengths are equal, and (b) stress levels are equal but opposite in sign on the upstream and downstream sides. Then, ϕ for the

API model would vary between 6.3 and 8.2 while for Ponter et al.'s it would vary between 3.7 and 7.3. For the artificial island considered earlier and other typical artificial islands with D/t>20, the behavior is closer to a plane stress condition. Both Model B and the API model tend to predict similar global pressures under this scenario.

ICE PRESSURES FOR NEW UNIAXIAL MODEL

The uniaxial behavior of sea ice has often been idealized with the power-law creep formulation. This model relates the strength of ice to the strain-rate, and as such is an incomplete description of the stress-strain-strainrate characteristics of the material. Several investigators have proposed more complete uniaxial models, some empirical in nature, that seem to be able to reproduce the post-peak decrease of stress in ice under constant strain-rate conditions. However, most of these models have not been fit to any specific data on sea ice. In addition, since they represent behavior only under constant strain-rate conditions, it is difficult to extend the models to other loading conditions such as constant stress (creep) and stress-rates.

A phenomenological approach based on simple thermorheological models is used here to develop a new uniaxial model, which is then calibrated with the sea ice data of Wang (10). This model applies equally well for constant stress-rate and creep conditions. In addition, under constant strain-rate conditions the strain at peak stress is a function of the strain-rate. The strength-strainrate relationship derived from the new uniaxial model is extended for multi-axial stress states and then applied to obtain indentation pressures.

New Uniaxial Constitutive Model.-- The new uniaxial constitutive model is based on the concept that the strength of an ice specimen is affected simultaneously by work or strain hardening and work softening or recovery. The latter phenomenon may occur due to recrystallization or micro-voids formation. This concept was used by Orowan (7) for examining steady state creep, and may be expressed as:

$$\frac{d\sigma}{dt} = \frac{\partial \sigma}{\partial \varepsilon} \dot{\varepsilon} + \frac{\partial \sigma}{\partial t} \qquad (15)$$

where $h=\partial\sigma/\partial\varepsilon$ is the coefficient of work hardening and $r=-\partial\sigma/\partial t$ is the rate of recovery. The parameter h is generally modelled as (6):

$$h = A \dot{\varepsilon}^{1/N} \exp(-M\varepsilon) \qquad (16)$$

where Q is the activation energy and R is the universal gas constant; A, N and M are the parameters of the equation. Due to a lack of general models for work softening, it is assumed here that the form is similar to that for work hardening:

$$r = B \dot{\varepsilon}^{1/K} \exp(-L\varepsilon) \qquad (17)$$

with B, K and L being the parameters of the equation. Substituting Eqs. (16) and (17) into Eq. (15) yields after integration (assuming $\dot{\varepsilon}$ and T are constant with $\varepsilon=\dot{\varepsilon}t$ and $\sigma=0$ at $t=0$):

$$\sigma = \left[\frac{A}{M} \dot{\varepsilon}^{1/N} \{1-\exp(-M\varepsilon)\} - \frac{B}{L} \dot{\varepsilon}^{1/K-1} \{1-\exp(-L\varepsilon)\} \right] \qquad (18)$$

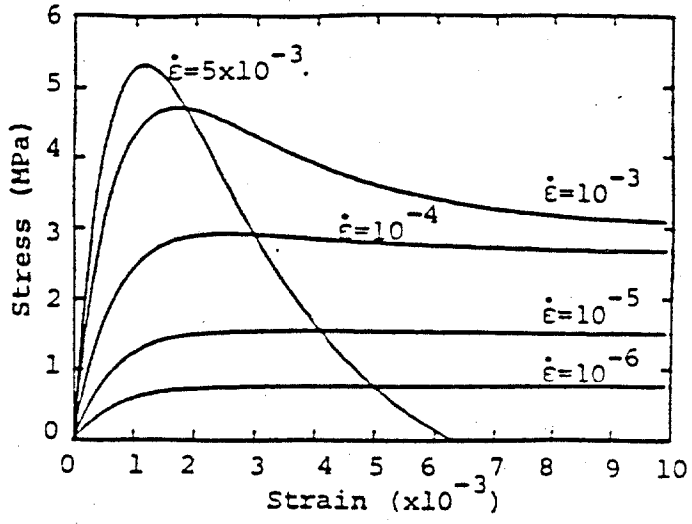

Fig. 3.--Stress-Strain Curves for Constant Strain-Rate Using New Model

The parameters of Eq. (18) obtained from Wang's (10) experimental data are: A=114025 MPa $s^{1/3}$, B=217408 MPa $s^{2/3}$, M=1411.2, L=430, N=3 and K=0.6. The stress-strain plots for the new model are shown in Fig. 3.

The two plots of the stress-strain behavior for $\dot{\varepsilon}=10^{-3}$ s^{-1} shown in Ref. 10 are vastly different, one shows strain softening behavior with resultant residual strength, while in the other the stress reduces to zero very sharply for strains exceeding the peak stress. The new model (Fig. 3) reflects this behavior for strain-rates of 10^{-2} - 10^{-3} s^{-1}, suggesting that the stress-strain behavior is very sensitive to strain-rate in this region.

Ice Pressure Prediction.-- The uniaxial model developed here relates the stress to strain and strain-rate. The strength-strainrate relationship derived from the model is extended for multi-axial stress states under the assumptions of isotropy and incompressibility made earlier for the power-law creep model. These assumptions are reasonable for the strain-rates of interest in this paper. Ice pressures obtained with this model can then be compared with the results for the power-law creep model. A general analysis strategy to incorporate the effect of strain and temperature is currently under development.

The strength-strainrate relationship for the new uniaxial model is plotted in Fig. 4 and compared with the power-law creep model. Notice that the new model predicts lower strength at strain-rates less than 10^{-5} s^{-1}, consistent with experimental data which suggests that the effective power-law exponent is an increasing function of strain-rate.

The new constitutive model can be viewed as the superposition of three power-law models of the type considered in the previous section and as such the local pressures will be distributed similarly. A typical order of magnitude global pressure for the artificial island considered here, based on Kinematic Model B and Eq. (13), is about 250 psi (1.7 MPa). This is only 70% of the pressure predicted by the power-law creep model. The 30% reduction in pressure is significant, although this reduces to approximately 10% when using Eq. (11). The pressure in the latter case is about 480 psi (3.3 MPa).

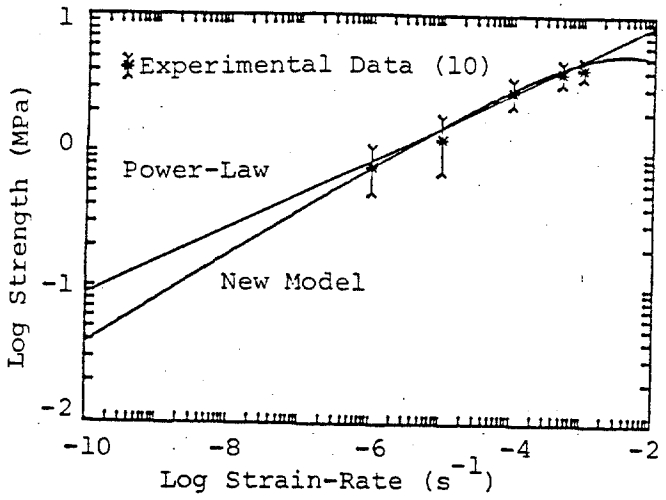

Fig. 4.--Comparison of Uniaxial Strength-Strainrate Relations

CONCLUSIONS

This study of global and local indentation pressures in the creeping mode of sea ice deformation, accounting for the spatial variation of strain-rates, leads to the following specific conclusions:

1. Kinematic Model B better models the ice movement survey data obtained from an artificial island in the Beaufort Sea than Kinematic Model A.
2. In the creeping mode of ice deformation, the local ice pressures are of the same order of magnitude as or lower than the global pressures. Even if the global pressures are reduced, e.g., by a factor of three, to account for scale (fracturing) effects, the local pressures based on the strain path method will only be 1.5 (and not three) times the upper bound global pressure neglecting interface friction.
3. Under essentially plane stress conditions, Kinematic Model B and the API model (1) predict similar global pressures. For a typical artificial island just prior to break-out with ice movements of less than 1 ft/hr (85×10^{-6} m s^{-1}), Model B predicts a pressure (neglecting interface friction) of approximately 530 psi (3.7 MPa).
4. The constitutive law based on the new uniaxial model predicts global pressures that are lower than that from the power-law creep model. For a typical artificial island, this reduction can be as much as 10-30 percent.

A key finding of this work is that for the rate-dependent material models describing sea ice behavior, interface adfreeze and friction stresses may significantly influence both local and global ice pressures. This has major economic consequences for platform design. Incorporation of these "non-conservative" stresses within the bound method may yield more accurate global ice pressures, but the solutions will not necessarily be upper bounds. More exact estimates of both local and global ice pressures using the strain path method may be

obtained by postulating kinematic models that more correctly model the interface conditions. However, currently available field data does not provide adequate resolution of the ice movements in the immediate vicinity of the structure to calibrate such models. In conclusion, it appears that the development of numerical models based on the finite and boundary element methods of analysis is necessary for more realistically studying ice-structure interaction problems where both global and local pressures are of interest.

ACKNOWLEDGEMENTS

The authors would like to thank Professors Jerome J. Connor and Mohsen M. Baligh for stimulating discussions during the course of this work. This research is funded by The Standard Oil Company (Ohio) through MIT's Center for Scientific Excellence in Offshore Engineering, and cosponsored by the U.S. Department of the Interior, Minerals Management Service.

APPENDIX.--REFERENCES

1. API Bulletin on Planning, Designing, and Constructing Fixed Offshore Structures in Ice Environments, Bul. 2N, First Edition, January, 1982.
2. Baligh, M.M., "The Strain Path Method in Geotechnical Engineering," Research Report R84-01, No. 761, Department of Civil Engineering, Massachusetts Institute of Technology, Cambridge, Massachusetts, 1984, 55p.
3. Bruen, F.J., and Vivatrat, V., "Ice Force Prediction Based on Strain-Rate Field," Third International Symposium on Offshore Mechanics and Arctic Engineering, New Orleans, LA, February 12-16, 1984, 7p.
4. Hill, R., "The Mathematical Theory of Plasticity," Oxford University Press, London, 1950, 355 p.
5. Hill, R., "A General Method of Analysis for Metal-Working Process," Journal of the Mechanics and Physics of Solids, Vol. 11, 1963, pp. 305-326.
6. Meyers, M.A. and Chawla, K.K., "Mechanical Metallurgy - Principles and Applications," Prentice-Hall Inc., Englewood Cliffs, New Jersey, 1984, 761 p.
7. Orowan, E. and Scott, J.W., "The Creep of Metals," Journal of Iron and Steel Institute, Vol. 54, 1946, p. 45.
8. Ponter, A.R.S. et al., "The Force Exerted by a Moving Ice Sheet on an Offshore Structure: Part I The Creep Mode," Cold Regions Science and Technology, Vol. 8, 1983, pp. 109-118.
9. Vivatrat, V., Chen, V., and Bruen, F.J., "Ice Load Prediction for Arctic Nearshore Zone," Brian Watt Associates, Inc., Texas, 1984, 26p.
10. Wang, Y.S., "Rate-Dependent Stress-Strain Relationship for Sea Ice," First International Symposium on Offshore Mechanics and Arctic Engineering, New Orleans, LA, 1982, pp. 243-248.

OTC 5056

SEA ICE INDENTATION IN THE CREEPING MODE

by Fadi S. Chehayeb, Seng-Kiong Ting, S. Shyam Sunder and Jerome J. Connor,
Massachusetts Institute of Technology

ABSTRACT

A finite element method of analysis is developed and applied to the study of global and local pressures generated on a cylindrical indenter during sea ice deformations in the creeping mode. Numerical simulations are performed under plane stress conditions to assess the influence of interface adfreeze and friction, material constants for a multi-axial power-law creep model, indenter diameter, and ice sheet velocity on predicted pressures. The results are compared with those based on approximate methods of analysis. Stress, strainrate and strain contours are obtained in addition to the distribution of interface pressures.

INTRODUCTION

Extraction of hydrocarbons from the Arctic offshore requires the design of drilling and production platforms to withstand loading generated by perennial ice features. Two levels of loading are typically considered; Global ice forces govern the overall structural geometry and dimensions as well as the foundation design while local pressures are likely to dictate wall thicknesses and local framing, and may well govern structural cost.

The interaction of an ice sheet with a vertically faced (and usually rigid) indenter is an important loading condition for cylindrical structures and for conical structures with grounded rubble pile or accreted ice foot. In general, this indentation phenomenon is characterized by the simultaneous occurrence of viscous (rate-dependent) and fracture behavior.

Several theoretical models based on approximate methods of analysis that idealize the ice sheet as a continuum have been proposed for predicting global ice forces. These include: (1) the upper and lower bound, plasticity type solutions of Michel and Toussaint[1], Croasdale et al.[2], and Ralston[3], (2) the reference stress, power law creep solution of Ponter et al.[4], and (3) the upper bound, power law creep solutions of Bruen, Vivatrat and Chen[5,6], and Ting and Shyam Sunder[7]. The plasticity type models require empirical definition of an average strain rate measure to account for the viscous behavior of ice, the reference stress approach accounts for the effect of variability in material constants in an approximate sense, and the upper bound, power law creep solutions require accurate specification of ice sheet kinematics. No equivalent theoretical models exist for the case where either pure (linear elastic) fracture or combined viscous and fracture effects dominate.

Theoretical predictions of interface pressures are not generally available. However, Ting and Shyam Sunder[7] have applied the (approximate) strain path method of analysis, originally developed for deep penetration problems in soil mechanics by Baligh[8], to study interface pressures during plane strain indentation. Their results for a power law creep model of ice showed that normal interface pressures may be 0.5-1 times the global pressure. They also found that interface adfreeze and friction stresses can significantly influence ice pressures.

The "continuum" predictions of ice pressures may in many cases be too high by a factor of 2-10. Four major factors can explain this uncertainty: (i) incomplete modeling of the mechanical behavior of ice, including temperature and fracture effects, (ii) empiricism in the theoretical models resulting from the use of approximate analysis methods, (iii) inadequate modeling of contact forces at the ice-structure interface, and (iv) ignoring the effects of size on material strength.

A study of ice indentation in the creeping mode is important for two reasons: (a) creep is the predominant mode of deformation for artificial islands in the Arctic nearshore region during "breakout" and/or steady indentation conditions occurring in the winter, and (b) stresses, strains, and strainrates within the continuum resulting from creep are necessary to predict the initiation and possibly even the propagation of cracks when viscous effects influence fracture behavior. In a recent paper, Shyam Sunder and Ting[9] have shown that a limiting tensile strain criterion dependent on the instantaneous strainrate can explain crack initiation in ice. Furthermore, for load transmitting systems such as ice features (as opposed to load bearing structural systems) the use of this criterion for fracture propagation is likely to be

References and illustrations at end of paper.

conservative when compared to a classical fracture mechanics approach. This is because the latter considers only the propagation of pre-existing cracks with a given distribution of sizes, while the former may be used to predict both the initiation and propagation of cracks in a material originally in virgin (flawless) form.

This paper is concerned with the development and application of a finite element method of analysis for studying global and local pressures generated on a rigid, cylindrical indenter during sea ice deformations in the creeping mode. Numerical simulations are performed under plane stress conditions to assess the influence of interface adfreeze and friction, material constants for a multi-axial power law creep model, indenter diameter, and ice sheet velocity on predicted pressures. The results are compared with those based on approximate methods of analysis. Stress, strainrate, and strain contours are obtained in addition to the distribution of interface pressures.

FINITE ELEMENT FORMULATION

Governing Equations.-- For general viscoplastic behavior, which includes creep, it is convenient to work with time derivatives of the governing equations for a solid. The weighted equilibrium-rate equation which forms the basis for the finite element displacement method is then given by:

$$\int \underline{B}^T \dot{\underline{\sigma}}\, dV = \dot{\underline{P}} \qquad (1)$$

where $\underline{B}$ is the strainrate - nodal velocity transformation matrix derived from the chosen displacement expansion for the finite element, i.e.,

$$\dot{\underline{\varepsilon}} = \underline{B}\,\dot{\underline{U}} \qquad (2)$$

The strainrate vector consists of two components, one due to elastic strains, characterized by the compliance matrix $\underline{C}$ and its inverse the rigidity matrix $\underline{D}$, and the other due to inelastic (irrecoverable) strains.

$$\dot{\underline{\varepsilon}} = \underline{C}\,\dot{\underline{\sigma}} + \dot{\underline{\varepsilon}}_I \qquad (3)$$

where I refers to the inelastic strains. For linearly elastic behavior, the compliance and rigidity matrices do not vary in time. The inelastic component may consist of rate-independent plastic strains, permanent creep (nonlinear viscoelastic) strains, and/or viscoplastic strains. In general, this may be expressed as:

$$\dot{\underline{\varepsilon}}_I = f(\underline{\sigma}, \dot{\underline{\sigma}}, \underline{\varepsilon}_I, T) \qquad (4)$$

where T allows for temperature dependence.

Combining Eqs. (1)-(3) and defining $\underline{K}$ as the elastic stiffness matrix of the element leads to the element equilibrium equation:

$$\underline{K}\,\dot{\underline{U}} = \dot{\underline{P}} + \int \underline{B}^T\,\underline{D}\,\dot{\underline{\varepsilon}}_I\, dV \qquad (5)$$

and the element stressrate - nodal velocity relations:

$$\dot{\underline{\sigma}} = \underline{D}\,\underline{B}\,\dot{\underline{U}} - \underline{D}\,\dot{\underline{\varepsilon}}_I \qquad (6)$$

The global stiffness matrix, $\underline{K}_G$, is obtained from Eq. (5) using conventional procedures.

Material Modeling.-- In this paper, sea ice is treated as a linearly elastic plus creeping material. Thus, $\underline{K}$ is the element stiffness matrix usually employed in linear elastic analyses. Under uniaxial (compressive) loading conditions, creep in ice is generally expressed in terms of a power law[10], i.e.,

$$\dot{\varepsilon}_c = a\,\sigma^N \qquad (7)$$

where a and N are constants with the temperature dependence being included in the parameter a following an Arrhenius activation energy law.

The multi-axial generalization of the creep law as proposed by Palmer[11] is based on assuming incompressibility, which is valid for ice as long as the hydrostatic stress is not too high such as under plane stress conditions. It suffices then to relate the creep strainrate tensor to the deviatoric stress tensor. This is accomplished by assuming that the two tensors are directly proportional to one another as given by the associative flow rule:

$$\dot{\underline{\varepsilon}}_c = \lambda\,\underline{S} \qquad (8)$$

where λ is a scalar parameter and $\underline{S}$ is a vector containing the deviatoric stresses. For a von Mises (isotropic) yielding surface, λ is the ratio of the octahedral shear strainrate to the octahedral shear stress. For the uniaxial power law given in Eq. (7), it follows that:

$$\lambda = 3/2\; a\; \sigma_e^{N-1} \qquad (9)$$

with the effective stress measure σ_e defined as:

$$\sigma_e = (3/2\; S_{ij}S_{ij})^{1/2} \qquad (10)$$

Given the stress vector, the deviatoric stresses may be obtained by subtracting the hydrostatic stress, i.e., $\underline{S}=\underline{G}\underline{\sigma}$ in matrix form. Then applying Eqs. (10), (9), and (8) in succession leads to the creep strainrate vector.

Solution Algorithm.-- An iterative solution algorithm is developed to solve a pseudo-force form of the nonlinear governing equations given in Eqs. (5) and (6). Although the algorithm has been applied to the specific material model presented above, it can be easily generalized to account for material anisotropy and for cracking based on the limiting tensile strain criterion. For purposes of discussion, attention is focussed at the element rather than the global level. At first the governing equations are integrated in time between t_i and t_{i+1} to yield:

$$\underline{K}(\underline{U}_{i+1}-\underline{U}_i) = \underline{P}_{i+1}-\underline{P}_i + \int \underline{B}^T\underline{D}(\underline{\varepsilon}_{c,i+1}-\underline{\varepsilon}_{c,i})\, dV \qquad (11)$$

$$\underline{\sigma}_{i+1}-\underline{\sigma}_i = \underline{D}\,\underline{B}(\underline{U}_{i+1}-\underline{U}_i) - \underline{D}(\underline{\varepsilon}_{c,i+1}-\underline{\varepsilon}_{c,i}) \qquad (12)$$

Creep strains which appear in both the equations are nonlinear functions of stress since λ in Eq. (8) is not a constant. A two-level interative algorithm is used to solve these equations for each new time step t_{i+1}. The key steps in the solution algorithm are as follows:

1. Compute the displacement increments from (the global form of) Eq. (11) for the given loading vector. In the first iteration on the equation, the incremental creep strains are assumed to be zero.

2. Compute the incremental stresses and incremental creep strains from Eq. (12) for the displacement increments obtained in step 1 using the iterative algorithm (lower-level iteration in k) discussed below. In the first iteration on this equation assume the incremental creep strains to be zero.

3. Return to step 1 and iterate on Eq. (11) (higher-level iteration in j) using the incremental creep strains obtained in step 2 until convergence is achieved. Two convergence criteria are used: (a) ratio of norm of displacement increment vector to norm of displacement vector at given time step is less-than-or-equal-to 0.001; and (b) absolute value of energy norm is less-than-or-equal-to 0.001, i.e.,

$$\left| \frac{\Delta \underline{P}^j \cdot \Delta \underline{U}^j}{\Delta \underline{P}^o \cdot \Delta \underline{U}^o} \right| \leq 0.001 \qquad (13)$$

where $\Delta \underline{P}$ refers to the entire right hand side of Eq. (11). The evaluation of the integral defining the inelastic load vector is based on a Gaussian quadrature formula (for a four-noded quadrilateral element, four integration points are used). Typically, 4-6 iterations are required for convergence at the higher-level.

The evaluation of the incremental stresses and incremental creep strains in step 2 requires the simultaneous consideration of Eqs. (12) and (8). In addition to a nonlinear equation solver, a numerical time integrator is needed to obtain results. Previous investigators[12,13,14] have used a simple successive substitution type algorithm to decouple the two equations. This involves the use of incremental creep strains from iteration k to evaluate the incremental stresses for iteration k+1 using Eq. (12). The incremental creep strains for iteration k+1 are then evaluated with the α-method of numerical time integration which expresses Eq. (8) as:

$$(\underline{\varepsilon}_{c,i+1} - \underline{\varepsilon}_{c,i}) = \lambda_\alpha \, \underline{S}_\alpha \, (t_{i+1} - t_i) \qquad (14)$$

where $\underline{S}_\alpha$ is a weighted average of the deviatoric stress vector in the time interval $(t_{i+1} - t_i)$ and λ_α is derived from a similar weighting on the effective stress, i.e.,

$$\underline{S}_\alpha = (1-\alpha) \, \underline{S}_i + \alpha \, \underline{S}_{i+1} \qquad (15)$$

Typical values of α lie in the range 0-1. A value of α equal to zero yields the forward (explicit) Euler method, while α equal to one yields the backward (implicit) Euler method. Both these formulas are first-order accurate (for linear problems in which λ is a constant, and not dependent on the effective stress), although the actual error of the backward formula is considerably less than that of the forward formula assuming that the former is iterated up to convergence. A value of α equal to 0.5 yields the well-known trapezoidal rule, also called the improved Euler's method since it is second-order accurate. A linear stability analysis of the α-method shows that it is unconditionally stable only for $\alpha \geq 0.5$.

For quasi-elastic problems in which creep deformations are not dominant, experience has shown that for small time increments $\alpha=0.5$ is more accurate, and that for large time increments $\alpha=1$ is to be preferred. However for creep dominant problems of concern here, the convergence rate slows down considerably for highly stressed elements when $\alpha=1$ is used, and more than 10-12 iterations may be needed for convergence at the lower-level. This is computationally unattractive since iteration is necessary at each integration point within an element (four in the case of a quadrilateral element) and highly stressed elements may occur often in a large finite element grid, e.g., consisting 250 elements.

Convergence is accelerated here by developing a lower-level algorithm that combines a Newton-Raphson or tangent type iteration with the α-method. The resulting equations are listed below:

$$\left[\underline{I} + \underline{D} \left[\frac{\partial \Delta \underline{\varepsilon}_c}{\partial \underline{\sigma}}\right]^k_{i+1}\right] \underline{\sigma}^{k+1}_{i+1} = \underline{\sigma}_i + \underline{D}\left[\underline{B}\Delta \underline{U} - \Delta \underline{\varepsilon}^k_c\right] + \underline{D}\left[\frac{\partial \Delta \underline{\varepsilon}_c}{\partial \underline{\sigma}}\right]^k_{i+1} \underline{\sigma}^k_{i+1} \qquad (16)$$

where $\Delta \underline{\varepsilon}_c{}^k$ is obtained by applying Eq. (14) after obtaining the stress quantities at iteration k, and similiarly:

$$\left[\frac{\partial \Delta \underline{\varepsilon}_c}{\partial \underline{\sigma}}\right]^k_{i+1} = \Delta t \, \alpha \left[\lambda \underline{I} + \frac{3}{2} \sigma_e^{-1} \frac{\partial \lambda}{\partial \sigma_e} \underline{S} \, \underline{S}^T\right]^k_\alpha \underline{G} \qquad (17)$$

For the given material model, $\partial\lambda/\partial\sigma_e$ can be obtained from Eq. (9). Notice that the algorithm becomes explicit for $\alpha=0$ as it should and no iteration is required. Convergence is defined to occur when the maximum absolute value of the relative change in point stresses between iteration k and k+1 is less-than-or-equal-to 0.001. Iteration is also stopped if the actual point stresses are zero at k and their maximum absolute value is less-than-or-equal-to 0.001 at k+1. Application of this iterative scheme with $\alpha=1$ shows that convergence is typically obtained in 4 iterations instead of more than 10-12, thereby cutting down the computational effort by approximately 50% if the increased computational effort per iteration is accounted for.

Computer Implementation.-- The finite element analysis algorithm has been implemented in a computer code called DECNEC (Discrete Element Computational NEtwork Controller). Data input is simplified by the use of a pre-processor specially written for the program. A post-processor called ORION, originally developed at the Lawrence Livermore Laboratory, can produce graphical display of stress, strain, and strainrate contours as well as interface pressure distributions.

The current implementation is a two-dimensional version for plane stress problems, while the development of a plane strain version is underway. A four-noded quadrilateral element is currently available. Although an eight-noded quadratic element is often preferred (and will be included in the future), accurate results can and have been obtained with the four-noded element using a finer finite element mesh. The program has the ability to simulate a free or frictional contact between two deformable bodies, i.e., no contact stresses due to adfreeze bond, by defining the interface as a "slideline".

Code Verification.-- The accuracy of the computer code has been verified in two ways; through the solution of simple test problems, and by comparing (see subsequent section) the variability in predicted global pressures due to indenter diameter, material model parameters, and ice sheet velocity with that predicted by approximate methods of analysis. In both cases, the numerical solutions are accurate to within specified tolerances typically achievable in finite element analyses.

One of the test problems, for example, considers a two-dimensional rectangular element subjected to a uniform compressive stress ($\sigma_z = -\sigma$) normal to one of its sides and with normal movement constrained on the other three sides (Fig. 1). A simple analysis shows that for the given material model, the lateral stress (σ_y) is given by:

$$\sigma_y = -\sigma_z/2 \left[(1-2\nu)e^{-2/3E\lambda t} - 1\right] \qquad (18)$$

where ν is the Poisson's ratio and E is the Young's modulus. This solution is valid for a constant value of λ, which in an average sense may be defined as its value at steady state. Under steady state conditions, i.e., large t, Eq. (18) shows that the lateral stress is compressive and equal to half the z-stress. Furthermore, the z-strainrate is the creep strainrate and equals $-1/2\ \lambda\sigma$ while the lateral strainrate is zero as it should be for the given boundary conditions. Application of DECNEC using two finite elements verified this analysis.

NUMERICAL SIMULATIONS

Description of Case Studies.-- Numerical simulations are performed for the seven cases identified in Table 1. The objectives of the first three simulations are to quantify the effect of interface adfreeze and friction on predicted indentation pressures. The fixed condition provides an upper bound solution since the ice-structure interface is considered to be infinitely strong. The free condition corresponds to no adfreeze bond and interface friction, while the roller condition provides an intermediate solution. The next two simulations study the influence of ice sheet velocity on pressures. The chosen base velocity of 0.195 m/hr corresponds to the recorded maximum average velocity over a twelve-hour period just prior to "breakout" (macrocracking) for an artificial island in the Beaufort Sea. The sixth simulation attempts to quantify the effect of a grounded rubble pile or an accreted ice foot on ice pressures by defining a larger effective indenter diameter (2.85 times the structural diameter). The final simulation studies the effect of variability in constants defining the material model on ice pressures. Two sets of parameters for sea ice based on the work of Sanderson[15] and Wang[16], respectively, are considered: N=3, $a=2.125\times10^{-6}$ $(MPa)^{-3}s^{-1}$; and N=4, $a=1.848\times10^{-6}$ $(MPa)^{-4}s^{-1}$. The elastic constants, which have negligible influence on the steady state solutions, are taken to be E=9.5 GPa and ν=0.3.

Numerical Implementation.-- Prior to carrying out the above studies, it is necessary to set up the finite element mesh, specify a time increment for the analysis, and define the excitation.

The finite element mesh is defined such that (i) the aspect ratio of each element is as close to one as possible, (ii) the scatter in stresses predicted by adjacent elements at their common boundary is less than 10%, and (iii) the boundary of the ice sheet is a circle whose extent is sufficient to simulate the infinite medium. The first criterion is maintained by the pre-processor which makes the radial length of each element equal to its arc length nearer the indenter. The second criterion is controlled by specifying the number of radial segments into which a quarter-plane may be divided. A value of nine is considered here (for an eight-noded element five or six may suffice). The last criterion is also implemented by the pre-processor which makes the radius of the circular boundary equal to 9.5 times the indenter radius. Accounting for symmetry about the z-axis, the above discretization leads to a finite element mesh with 252 elements and 285 nodal points (Fig. 2). The number of degrees-of-freedom is 476 for the fixed condition, 538 for the roller condition, and 540 for the free condition.

The choice of time increment is made to satisfy the conflicting requirements of accuracy and computational effort. Accuracy, in turn, is achieved by allowing sufficient time for the solution to reach steady state and by specifying a time increment that captures the variability in response prior to reaching steady state. Experience with the simulations has shown that it is appropriate to consider a time increment which makes the exponent in Eq. (18) equal to 40 in 20 time steps. For typical values of λ and E, the time increment is approximately 100 s.

The chosen uniform far-field velocity listed in Table 1 defines the excitation here, although other types of excitation such as environmental traction on the ice sheet can be handled equally well. For a given time step, the excitation is defined in terms of an imposed displacement in the z-direction at the far-field boundary nodes. This displacement value is made to increase linearly in time, consistent with the chosen uniform velocity.

DISCUSSION OF RESULTS

Global Forces.-- Table 2 lists the global pressures predicted by the finite element analysis for the seven cases of interest. Pressure values are the global forces divided by the indenter diameter D, and ice sheet thickness t.

Comparing the first three values of global pressure it is seen that the fixed condition does provide an upper bound solution. The global pressure for the fixed case is about 28% higher than that for the roller case. In turn, the global pressure for the roller case is 1.93 or almost twice that for the free case. This spread in global pressures is indicative of the influence of interface friction and adfreeze bond. The hundred percent reduction in pressure between the roller and free case can be explained by examining the stresses within the ice sheet. For the roller case, the upstream and downstream stresses are equal in magnitude and their resultants act together in the z-direction. In the free case, the downstream stresses are almost zero since the lack of contact at the interface on this side tends to eliminate any influence of the indenter on the ice sheet. As a result, the downstream part of the ice sheet acts predominantly like a rigid body. This tends to reduce global pressures by almost a half.

The fourth and fifth values of global pressure indicate that reducing the ice sheet velocity by a factor of 6.4 leads to a 46% reduction in pressures

while increasing the velocity by a factor of 1.6 leads to a 17% increase in pressures. Thus even a factor of two uncertainty in velocity will affect the pressures only by about 20-30%.

Cases 2 and 6 provide some idea of the effect of a grounded rubble pile or an accreted ice foot. By defining an effective indenter diameter equal to 2.85 times the structural diameter, the global pressure has reduced by 31%. However, the global force has actually increased by 97% from 211 MN/(unit ice thickness) for case 2. Two extreme scenarios can be considered to estimate the global force felt by the structure when there is a grounded rubble pile: (i) the entire global force is transmitted to the structure which in turn transmits it to the foundation, and (ii) both the structure and the grounded rubble pile resist the global force, each transmitting to the foundation a force proportional to its contact area with the foundation. Under the first scenario, which is probably overconservative, the global force on the structure is 414 MN/(unit ice thickness) an increase of 97% from case 2. Under the second scenario, which may be reasonable only if the rubble pile is consolidated and grounded firmly in the foundation soil such as in the case of constructed ice packs, the global force on the structure is 51 MN/(unit ice thickness) a reduction of 76% from case 2. Further research is necessary to quantify the level of force that can be directly transmitted to the foundation by a grounded rubble pile.

The last case shows that the two sets of material constants considered in this paper lead to ice pressures which differ by about 19%. Combining this information with earlier experience indicates that uncertainties in material constants for an isotropic power law creep model may yield ice pressures that vary by about 15-30%. However, improved material models that include fracture and temperature effects in addition to the transversely isotropic behavior of sheet ice can have a major influence on ice pressure predictions.

Calibration with Approximate Solutions.-- The global pressures for cases 4 through 7 indicate the influence of ice sheet velocity V, indenter diameter D, and material constants a and N on the results. In order to provide perspective and calibration with solutions based on approximate methods of analysis, the upper bound solution of Ting and Shyam Sunder[7] corresponding to a two-dimensional velocity field obtained by superposing a uniform flow and a doublet, is considered. The resulting kinematic model resembles the flow of an infinite ice sheet past a circular indenter with the interface matching most the roller condition. According to the solution, the global pressure is proportional to $(V/D)^{1/N}$. If this variation is valid, the ratio of global pressures in cases 4 through 6 to case 2 should be 0.54, 1.16 and 0.70, respectively. The finite element analysis predicts the ratios to be 0.54, 1.17 and 0.69. For the two sets of material constants in cases 7 and 2, the approximate solution predicts a ratio of 1.17 while the finite element analysis predicts a ratio of 1.19. In all cases, the effect of changes in V, D, a and N on the finite element solutions is almost identical to that predicted by the upper bound, creep law solution.

In order to compare the actual (as opposed to ratios of) global pressures, it is necessary to recognize that the two-dimensional nature of the chosen kinematic field makes the approximate analysis strictly correspond to a plane strain condition and not a plane stress condition. Ponter et al.'s[4] analysis for both plane strain and plane stress based on the reference stress method can be used to derive a correction factor by which to divide the approximate solution for applying it under plane stress conditions. For the material model with N=3 the correction factor is 1.8 and for the N=4 model it is 1.96. The approximate formula corrected by a rounded factor of 2 is given below:

$$\frac{P}{Dt} = \frac{2\pi}{\sqrt{3}} \frac{N}{N+3} \left[\frac{4}{\sqrt{3}} \frac{1}{a} \frac{2V}{D}\right]^{1/N} \qquad (19)$$

where the quantity in brackets raised to the power of 1/N may be interpreted as the uniaxial strength of ice evaluated at an average effective strainrate of $8/\sqrt{3}$ V/D using Eq. (7). Table 2 shows that the predictions based on Eq. (19) differ from the finite element solutions by less than 10%. The fixed condition is obtained by multiplying the above equation by 1.3, while the free condition uses a multiplying factor of 0.5 (Table 3). Note that (i) the uncorrected upper bound solutions are overconservative by almost hundred percent or more, and (ii) the approximate solutions need no longer be upper bounds once the correction factor is applied.

Local Pressures.-- The maximum (peak) interface normal stress for each of the seven simulations is listed in Table 2. The table also lists a maximum interface shear stress of 0.73 MPa for the fixed condition. There are no interface shear stresses for the roller and free conditions. Notice that in all cases the maximum normal pressure is approximately 0.35-1.10 times the global pressure, and not several (e.g., three) times the global pressure.

The maximum normal stress for the fixed condition is lower than that for the roller condition by 17%, although a reverse trend is observed for global pressures. This occurs because part of the force in the fixed condition is carried by interface shear stress. On the other hand, the maximum normal stress for the free condition is about 4% higher than that for the roller condition. There are no interface stresses on the downstream side for the free condition due to lack of contact between the ice sheet and the indenter. The small level of stresses that exist in the predominantly rigid continuum on the downstream side are transmitted to the structure from the upstream side, thereby increasing the normal stresses on that side by the 4% mentioned above.

Comparison of the local and global pressures shows that the ratio of the maximum normal interface stress to the global pressure is approximately 0.35 for the fixed condition, 0.55 for the roller condition, and 1.10 for the free condition. Furthermore, the variation of local pressures with V, D, a and N is similar to that for global pressures. Thus multiplication of Eq. (19) by 0.46, 0.55, and 0.55 can be used to estimate the respective maximum normal pressures (Table 3). In a similar fashion, the maximum interface shear stress for the fixed condition may be estimated from the equation with a multiplication factor of 0.37.

For purposes of design it is necessary to consider not only the maximum values of normal stress but also its distribution on the structure. The design of

individual structural components is typically based on a tributary loaded area. It is possible that the average integrated stress on this area due to contact with the ice sheet is significantly less than the point maxima of stress. Further, the average stress may reduce for structural components which have larger tributary areas. Figures 3 and 4 present the normal stress distributions on the interface. Note that the normal stresses are always zero where the indenter is tangential to the direction of ice sheet movement (i.e., angle equal to zero degrees). At the end of the first time step where the solution is predominantly elastic, the distributions are cosinusoidal as one may expect. However as steady state is reached, there is a tendency for the distributions to become rectangular or uniform. The distribution is more rectangular for the free and roller conditions than for the fixed condition which appears to be predominantly consinusoidal due to lower stress levels, as well as for the N=4 case than for the N=3 case since an increasing value of N makes the ice behave more like a rigid-plastic material. The figures also show that downstream interface stresses are zero for the free condition. The distributions are not affected, at least visually, as V and D are varied, although they have to be scaled according to the maximum normal stresses in Table 2. A conservative design approach may be to assume a uniform distribution of stresses based on the maximum normal interface stress.

A careful consideration of the interface stress levels sheds some light on which of the three conditions, fixed, roller or free, is realistic. Figure 5 shows the distribution of interface shear stresses for the fixed condition. At steady state, the distribution is predominantly sinusoidal with the maximum value of 0.73 MPa occurring at the tangent point. The shear strength of adfreeze bond and sea ice as reported in the literature[17,18] varies over a wide range 0.02-1.38 MPa. It is very likely that either the adfreeze bond will give way or the ice will fracture in shear over a significant fraction of the indenter perimeter. In addition, for the typical range of effective strainrates close to the downstream tip of the indenter, the tensile strength of ice is less than the downstream normal interface stresses for the fixed and roller conditions, both of which are tensile. Once again, if the adfreeze bond does not give way, a tensile fracture may occur in the ice over the perimeter close to the interface on the downstream side. Thus, for local pressures the use of the free condition should be preferred. The choice will be conservative over the fixed condition and, marginally so, over the roller condition. However, the free condition may be unconservative for global pressures if the indentation problem is one in which the structure is surrounded by an infinite ice sheet and it is possible for frictional stresses or adfreeze bond to develop at the interface.

Comparison with Pressure-Area Curves.-- Pressure-area curves are often constructed to help designers obtain the average pressures over tributary loaded areas for structural components[19]. A typical curve developed by Sanderson[20] is shown in Fig. 6. The darkly shaded areas on the figure correspond to actual measurements of ice pressure under widely varying conditions, while the lightly shaded areas represent the author's extrapolation of the measurements. The dark regions in the extreme left are from laboratory indentation tests such as those of Frederking and Gold[21], and Michel and Toussaint[1]. The central region reflects measurements from ice breakers traveling in the Arctic, while the two smaller regions on the right correspond to global forces on artificial islands estimated from pressure sensor measurements in the ice sheet. The contact area is defined as the indenter area of contact for the laboratory and artificial island data. For the ice breaker data, the contact area is the local area over which the pressure measurement is made and not the form area of the ice breaker. This figure shows that for an artificial island with a contact area of 200 m^2, the indentation pressure may be around 1 MPa. However for a local area of 10 m^2 on the same structure, the indentation pressure may be around 3 MPa.

The local to global pressure ratio of three obtained from the pressure-area curve seems to contradict the findings in the previous subsection. Fortunately, this is not so. If the contact area in Fig. 6 is interpreted as Dt, then a smaller contact area implies a smaller indenter diameter if the ice thickness remains unchanged. The effect of indenter diameter is well modelled by Eq. (19). A plot of the maximum normal interface pressure estimate from the equation leads to the solid line in the figure. Eq. (19) is appropriately modified to account for transition from plane stress to plane strain using Ponter et al.'s reference stress method[4]. This affects the curve, in an insignificant manner, over the region 1-10 m^2. When the effective strainrate, i.e., $8/\sqrt{3}\ V/D$, exceeds $5\times10^{-4}\ s^{-1}$, ice is assumed to have fractured (crushed) and the uniaxial strength is capped, leading to the flat portion of the curve on the extreme left. The predicted behavior provides an excellent match to Fig. 6. Thus, a more appealing interpretation of the figure is to consider the contact area as the indenter area (Dt in our case) and not the tributary loaded area for a structural component, and the indenter pressure corresponding to a given contact area as the maximum normal interface pressure for that indenter. The distribution of the interface stresses may be assumed uniform over the indenter area of contact as concluded earlier. However, a different boundary value problem involving a smaller contact area, as opposed to contact over half the perimeter in the free condition, will lead to higher interface pressures.

The key assumption in generating the analytical curve in Fig. 6 concerns the choice of V. The value of 0.195 m/hr considered here is based on data for an artificial island just prior to "breakout" or macrocracking, which leads to an excellent match between predicted and measured indentation pressures for the structure. However, significantly higher velocities do occur in the field for which the current predictive models based purely on an isotropic creep law will lead to increasing pressures. Fracture in ice will be the key mechanism that limits pressures generated under higher velocities.

Multiaxial Behavior of Ice Sheet.-- A study of the multiaxial behavior of an ice sheet during indentation in the creeping mode provides clues to likely failure modes, particularly fracture. All forms of fracture (crushing, spalling, splitting) initiate as a result of tensile strains perpendicular to the crack direction. Even if the applied loads at the element level are not tensile, it is possible for tensile conditions to occur in a rotated frame of reference, e.g., a 45° rotation in the case of pure shear.

Table 4 lists the principal stresses at the point of maximum interface pressure at two time instants: at the end of the first time step (around 100 s) where

the solution is predominantly elastic, and at the twentieth time step (around 2000 s or 30 minutes) where the solution has reached steady state and is predominantly creep. The biaxial stress state at the first time step is compression-tension for all the cases except for a fixed condition where it is compression-compression. As creep starts to dominate, all the cases tend to compression-compression. Figures 7 and 8 shows how this compression-compression region grows in time for the fixed and free cases. The region is much larger for the fixed condition than for the free condition. The roller condition is somewhere in between although it resembles more the free condition. The most striking observation that can be made from these figures is that tensile stresses occur almost all over the ice sheet. Biaxial tension tends to occur on the downstream side, while compression-tension states of stress are present on both sides. Experimental evidence under compression-tension states of stress[22] shows that the occurrence of even small tensile stresses weakens ice considerably, leading to premature fracture when compared with uniaxial tensile loading.

Figure 9 shows the strain fields, which are more relevant to explaining fracture initiation. Since the algebraically maximum principal strains are positive (or almost so) over the entire ice sheet for the fixed and roller conditions at steady state, there is no compression-compression (and by symmetry no tension-tension) region of strain. A tension-compression state of strain dominates the ice sheet, with tensile strains exceeding 0.001 at steady state. As the tensile failure strain is about 0.001 or less for strainrates greater than 10^{-7} s^{-1} under just uniaxial loading, it seems likely that cracking will occur even before steady state creep is reached. Similar conclusions apply for the free condition, the only difference being that downstream strains are negligible.

The maximum effective strainrates for the seven simulations are listed in Table 2. For the kinematic model considered by Ting and Shyam Sunder[7] which is closest to the roller condition, the maximum effective strainrate equals $8/\sqrt{3}$ V/D. The prediction of 2.3×10^{-6} s^{-1} for case 2 compares well with the finite element analysis value of 3.4×10^{-6} s^{-1}. Further, cases 4 through 6 are consistent with the predicted proportionality to V/D. Contours of effective strainrate are plotted in Fig. 10. The strainrates tend to zero at the tangent points for the roller and free conditions as one may expect and is a maximum close to but not at the tips. On the other hand, the tangent point has the maximum value for the fixed condition. In the immediate vicinity of the indenter, these plots are different from the circular contours predicted by the kinematic model in the approximate analysis. This finding reinforces Ting and Shyam Sunder's[7] observation that the approximate upper bound analysis is quite accurate for global pressures, although the use of the strain path method with a kinematic model that does not capture interface conditions may be inadequate for local pressure predictions.

CONCLUSIONS

This paper has presented a finite element method of analysis for studying the problem of sea ice indentation in the creeping mode of deformation. The analysis strategy, applicable to general viscoplastic behavior including creep (nonlinear viscoelasticity), is based on a secant type iteration involving 4-6 cycles per time step on the global equations of motion and a Newton-Raphson or tangent type iteration, combined with the α-method of time integration and typically not exceeding 4 cycles per time step, on the rate-dependent constitutive relations at each integration point within an element. The resulting computer code, called DECNEC, is capable of simulating a free or frictional contact between two deformable bodies, i.e., no contact stresses due to adfreeze bond, by defining the interface as a "slideline".

Numerical simulations of ice-structure interaction for a rigid cylindrical indenter under plane stress conditions, a problem of general interest for structural concepts in the Arctic, and an isotropic (von Mises) multi-axial power law creep model for sea ice showed that:

1. Global forces vary by a factor of 2.5 depending upon whether the interface condition is fixed (infinite adfreeze bond strength), roller, or free (no adfreeze bond strength or interface friction). The fixed condition is about 1.3 times and the free condition about 0.5 times the roller condition.

2. Finite element analysis predictions of global pressure differ from a (approximate) modified upper bound solution of Ting and Shyam Sunder[7] by less than 10% for varying velocity, indenter diameter, and material constants.

3. The ratio of maximum normal interface pressure to global pressure approximately varies in the range 0.35-1.10 depending upon the interface condition. It is 0.35 for the fixed condition, 0.55 for the roller condition, and 1.10 for the free condition.

4. The maximum (peak) normal interface pressures vary by a factor of 1.26 depending upon the interface condition. The fixed condition is about 0.83 times and the free condition about 1.04 times the roller condition. The maximum interface shear stress for the fixed condition is about 0.81 times the corresponding maximum normal pressure. However, a different boundary value problem involving a smaller contact area, as opposed to contact over half the perimeter in the free condition, will lead to higher interface pressures.

5. Pressure-area curves should be considered as providing the maximum normal interface pressure for a given indenter area of contact (form area), rather than the average integrated normal pressure over a tributary loaded area for a structural component. It is conservative to assume a uniform or rectangular distribution of the local pressure over the indenter area of contact for purposes of design.

6. Tensile stresses, strains and strainrates occur almost all over the ice sheet, and may be the key to explaining fracture behavior during indentation. While biaxial compression and tension states tend to occur for stress on the upstream and downstream sides, respectively, the state of strain is almost always compression-tension. The levels of

tensile strain are often sufficient to cause cracking even before steady state creep is reached.

The possible effect of a grounded rubble pile or accreted ice foot on ice pressures was assessed by defining an effective indenter equal to a multiple (2.85) of the structural diameter. This resulted in a factor of 1.97 increase in global force. In the case of a grounded rubble pile, it would be overconservative to consider that all this force is transmitted to the foundation by the structure. On the other hand, the force transmitted to the foundation by the structure would decrease by a factor of 4.14 if both the structure and the grounded rubble pile could transmit a force proportional to the contact area of each with the foundation. This may be reasonable only if the rubble pile is consolidated and grounded firmly in the foundation soil such as in the case of constructed ice packs. Further research is necessary to quantify the level of force that can be directly transmitted to the foundation by a grounded rubble pile.

The numerical simulations also showed that (i) even a factor of two uncertainty in velocity will affect ice pressures only by about 20-30%, and (ii) uncertainties in material constants for an isotropic power law creep model may yield ice pressures that vary by about 15-30%. However, improved material models that include fracture and temperature effects in addition to the transversely isotropic behavior of sheet ice can have a major influence on ice pressure predictions. In particular, fracture in ice will be the key mechanism that limits ice pressures generated under the significantly higher velocities that occur in the field when compared with the value just prior to "breakout" or macrocracking considered here. This is an area for further research.

NOMENCLATURE

a	constant parameter in power law
$\underline{B}$	transformation matrix
$\underline{C}$	finite element material compliance matrix
D	diameter of structure
$\underline{D}$	elastic rigidity matrix
E	Young's modulus
$\underline{G}$	transformation matrix for relating $\underline{S}$ to $\underline{\sigma}$
$\underline{K}$	elastic stiffness matrix of finite element
$\underline{K}_G$	global stiffness matrix
N	power law exponent
P	global force acting on structure
$\underline{P}$	applied load vector
$\underline{S}$	deviatoric stress vector
T	temperature
t	time or ice thickness
$\underline{U}$	nodal displacement vector
V	approach velocity of ice sheet
α	parameter in time integrator
$\underline{\varepsilon}$	total strain vector
$\underline{\varepsilon}_I$	inelastic strain vector
$\underline{\varepsilon}_c$	creep strain vector
λ	associative flow rule constant
ν	Poisson's ratio
σ_e	effective stress meassure
$\underline{\sigma}$	stress vector
$\dot{}$	rate form is represented by a dot above the symbol

ACKNOWLEDGEMENTS

This research is funded by the Standard Oil Company (Ohio) through MIT's Center for Scientific Excellence in Offshore Engineering, and cosponsored by the U.S. Department of the Interior, Minerals Management Service. The authors thank Jaideep Ganguly, graduate student, for computational assistance.

REFERENCES

1. Michel, S. and Toussaint, N., "Mechanisms and Theory of Indentation of Ice Plates," Journal of Glaciology, Vol. 19, No. 81, 1977, pp.285-300.

2. Croasdale, K.R., Morgenstern, M.R. and Nuttall, J.B., "Indentation Tests to Investigate Ice Pressures on Vertical Piers," Journal of Glaciology, Vol. 19, No. 81, 1977, pp.310-312.

3. Ralston, T.D., "An Analysis of Ice Sheet Indentation," IAHR Ice Symposium, Lulea, Sweden, 1978, pp.13-31.

4. Ponter, A.R.S. et al, "The Force Exerted by a Moving Ice Sheet on an Offshore Structure: Part I The Creep Mode," Cold Regions Science and Technology, Vol. 8, 1983, pp. 109-118.

5. Bruen, F.J. and Vivatrat, V., "Ice Force Prediction Based on Strain-Rate Field," Third International Symposium on Offshore Mechanics and Artic Engineering, New Orleans, LA, 1984, 7 p.

6. Vivatrat, V. and Chen, V.L., "Ice Load Prediction with the Use of a Rate-Dependent Anisotropic Constitutive Law," Proc. of the ASCE Specialty Conference: Arctic '85 - Civil Engineering in the Arctic Offshore, San Francisco, California, March 1985, 11p.

7. Ting, S-K. and Shyam Sunder, S., "Sea Ice Indentation Accounting for Strain-Rate Variation," Proc. of the ASCE Specialty Conference: Arctic '85 - Civil Engineering in the Arctic Offshore, San Francisco, California, March 1985, 11p.

8. Baligh, M.M., "The Strain Path Method," Research Report R84-01, No. 761, Department of Civil Engineering, Massachusetts Institute of Technology, Cambridge, Massachusetts, Jan. 1984, 47 p.

9. Shyam Sunder, S. and Ting, S-K., "Ductile to Brittle Transition in Sea Ice under Uniaxial Loading," Proc. of the 8th International Conference on Port and Ocean Engineering under Arctic Conditions, Narssarssuaq, Greenland, Sept. 1985, 12 p.

10. Glen, J.W., "The Creep of Polycrystalline Ice," Proc. of the Royal Society of London, Ser. A, Vol. 228, No. 1175, 1955, pp.519-538.

11. Palmer, A.C., "Creep-Velocity Bounds and Glacier-Flow Problems," Journal of Glaciology, Vol. 6, No. 46, 1967, pp.479-488.

12. Snyder, M.D. and Bathe, K.J., "A Solution Procedure for Thermo-Elastic-Plastic and Creep Problems," Nuclear Engineering and Design, Vol. 64, 1981, pp. 49-80.

13. Hughes, T.J.R. and Taylor, R.L., "Unconditionally Stable Algorithms for Quasi-Static Elasto/Visco-Plastic Finite Element Analysis," Computer and Structures, Vol. 8, 1978, pp. 169-173.

14. Krieg, R.D., "Numerical Integration of Some New Unified Plasticity-Creep Formulations," SMIRT-4, M6/4, 1977.

15. Sanderson, T.J.O., "Theoretical and Measured Ice Forces on Wide Structures," Proc. 7th International Symposium on Ice, IAHR, Hamburg, August 1984, 32p.

16. Wang, Y.S., "A Rate-Dependent Stress-Strain Relationship for Sea Ice," First International Symposium on Offshore Mechanics and Artic Engineering, New Orleans, 1982, pp. 243-248.

17. Gershunov, E.M., "Shear Strength of Adfreeze Bond and its Effect on Global Ice Load Applied to Mobile Offshore Drilling Units Under Artic Conditions," Offshore Technology Conference, Paper OTC 4687, 1984, pp. 357-362.

18. Oksanen, P., "Friction and Adhesion of Ice," IAHR Ice Symposium, Quebec, Canada, 1981, pp.628-640.

19. Bruen, F.J., Byrd, R.C., Vivatrat, V. and Watt, B.J., "Selection of Local Design Ice Pressures for Arctic Systems," Offshore Technology Conference, Paper OTC 4334, 1982, pp. 417-435.

20. Sanderson, T.J.O., Personal Communications, 1984.

21. Frederking, R. and Gold, L.W., "Experimental Study of Edge Loading of Ice Plates," Canadian Geotechnical Journal, Vol. 12, No. 4, 1975, pp. 456-463.

22. Haynes, F.D., "Tensile Strength of Ice under Triaxial Stresses," USA CRREL Research Report 312, 1973, 21 p.

TABLE 1 - SUMMARY OF CASES

Case	Velocity (ft/hr)	Diameter (ft)	N	Interface Condition
1	0.64	350	3	Fixed
2	0.64	350	3	Roller
3	0.64	350	3	Free
4	0.10	350	3	Roller
5	1.00	350	3	Roller
6	0.64	1000	3	Roller
7	0.64	350	4	Roller

Note: 1 ft = 0.3048 m

TABLE 2 - SUMMARY OF RESULTS

Case	P/Dt (MPa)		Maximum Interface Normal Stress (MPa)	Maximum Effective Strainrate (s^{-1})
	Finite Element Analysis	Modified Upper Bound		
1	2.54	2.44	0.90	4.0×10^{-6}
2	1.98	1.87	1.08	3.4×10^{-6}
3	1.02	0.94	1.13	4.0×10^{-6}
4	1.07	1.01	0.59	5.5×10^{-7}
5	2.31	2.18	1.28	5.5×10^{-6}
6	1.36	1.32	0.76	1.1×10^{-6}
7	2.34	2.20	1.27	4.5×10^{-6}

Note: Maximum Interface Shear Stress for Fixed Condition is 0.732 MPa
1 MPa = 145 psi

TABLE 3 - MULTIPLYING FACTORS FOR APPROXIMATE MODEL (Eq. 19)

Condition	Global Pressure	Maximum Interface Normal Stress
Roller	1.0	0.55
Fixed	1.3	0.46
Free	0.5	0.55

Note: Factor for Maximum Interface Shear Stress in Fixed Condition = 0.37

TABLE 4 - PRINCIPAL STRESSES AT UPSTREAM TIP OF INDENTER

Case	Elastic (Time Step 1)		Steady State Creep (Time Step 20)	
	σ_z(MPa)	σ_y (MPa)	σ_z(MPa)	σ_y(MPa)
1	-0.19	-0.07	-0.90	-0.39
2	-0.30	+0.07	-1.08	-0.16
3	-0.36	+0.10	-1.13	-0.16
4	-0.18	+0.04	-0.59	-0.09
5	-0.35	+0.08	-1.28	-0.20
6	-0.11	+0.03	-0.76	-0.10
7	-0.31	+0.08	-1.27	-0.26

Note: Tension is Positive
1 MPa = 145 psi

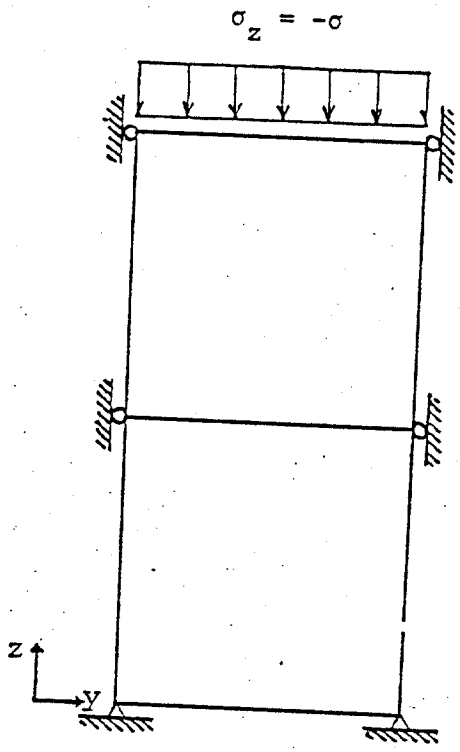

Fig. 1 - Test Problem

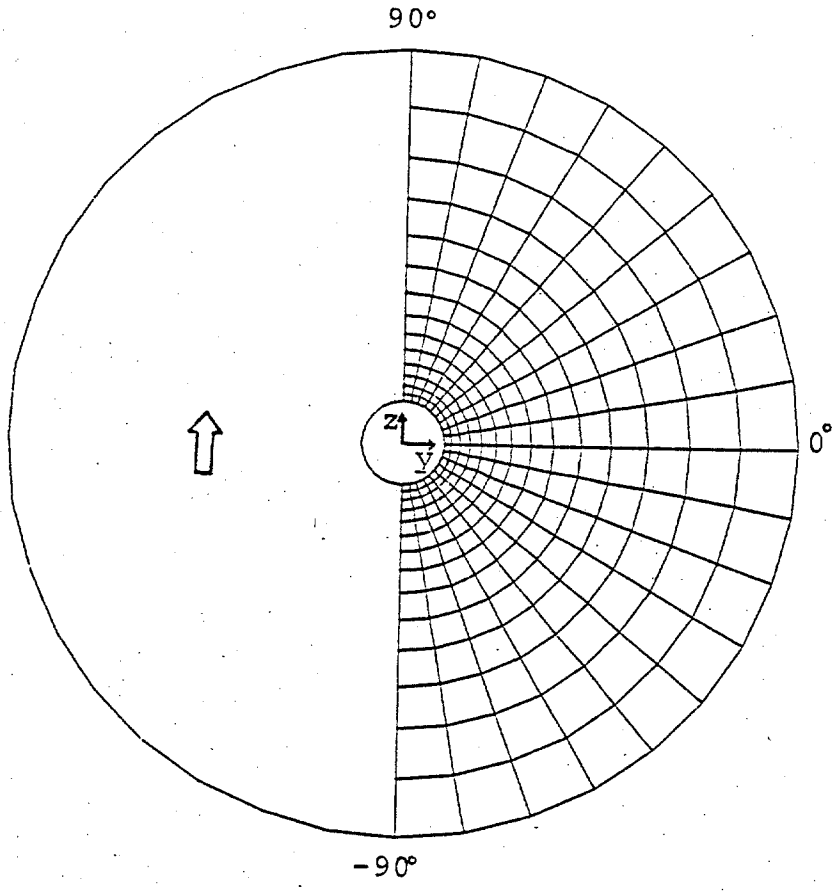

Fig. 2 - Finite Element Grid

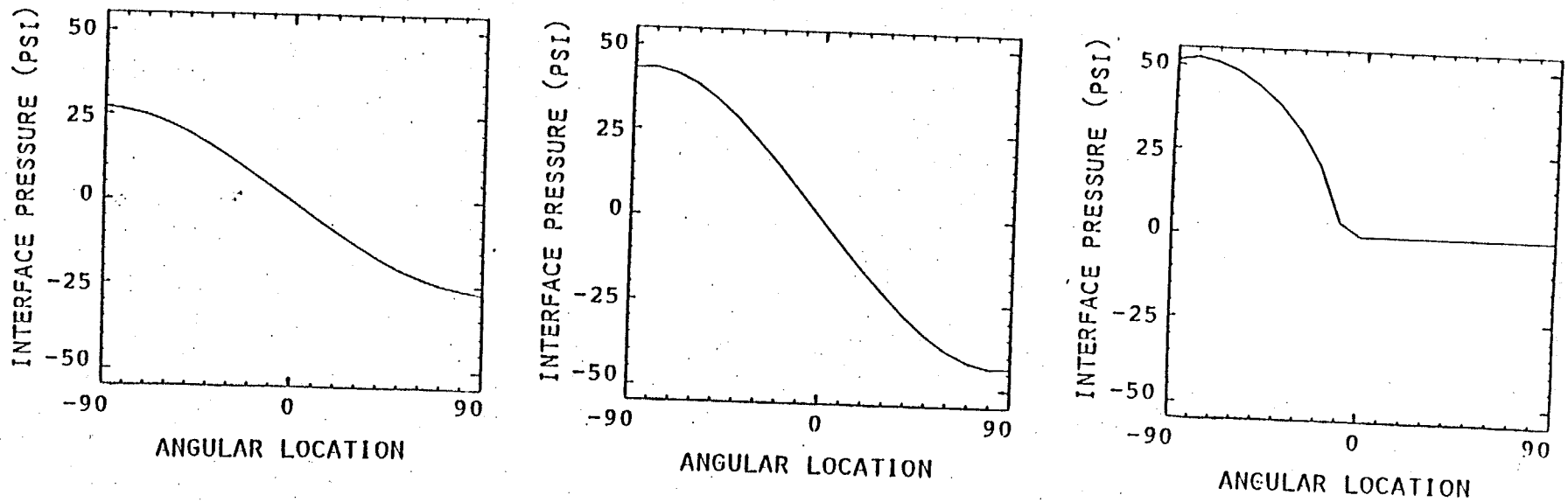

(a) Fixed Condition

(b) Roller Condition

(c) Free Condition

Fig. 3 - Normal Stress Distribution on Interface (Time Step 1)

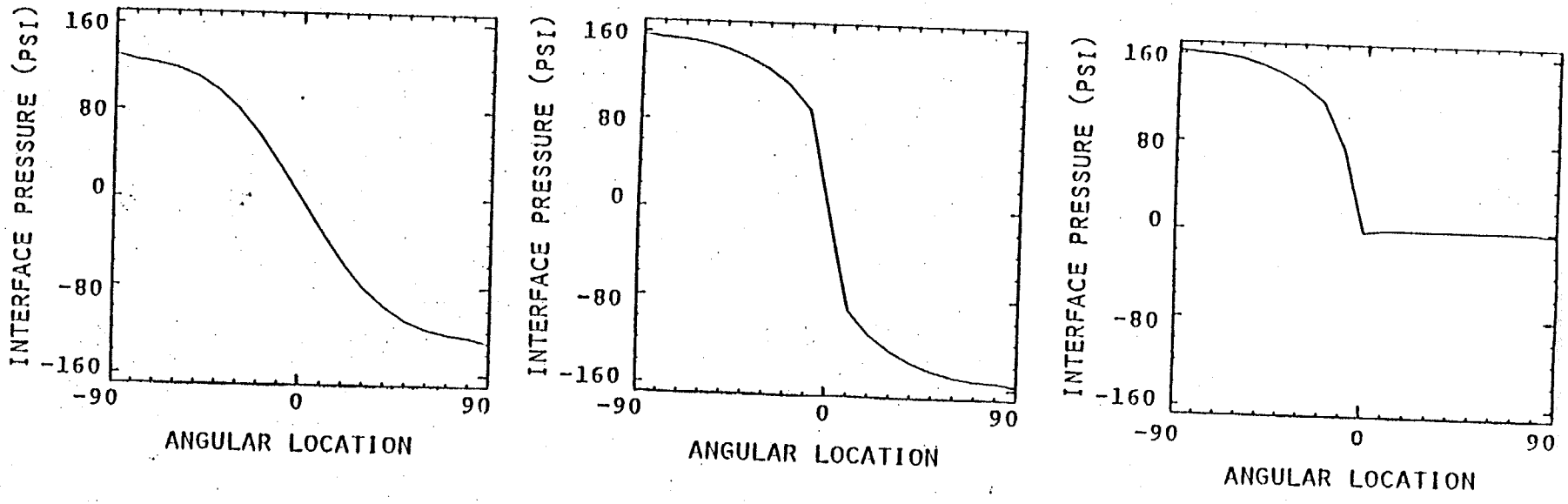

(a) Fixed Condition

(b) Roller Condition

(c) Free Condition

Fig. 4 - Normal Stress Distribution on Interface (Time Step 20)

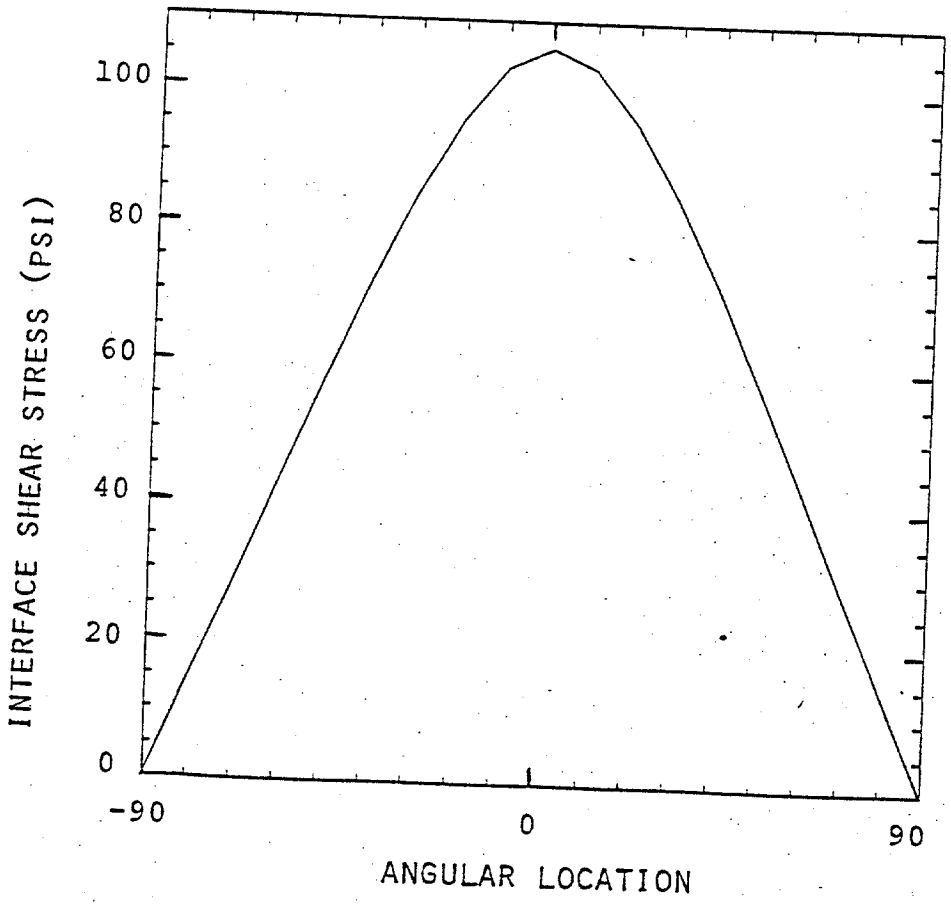

Fig. 5 - Shear Distribution on Interface for Fixed Condition (Time Step 20)

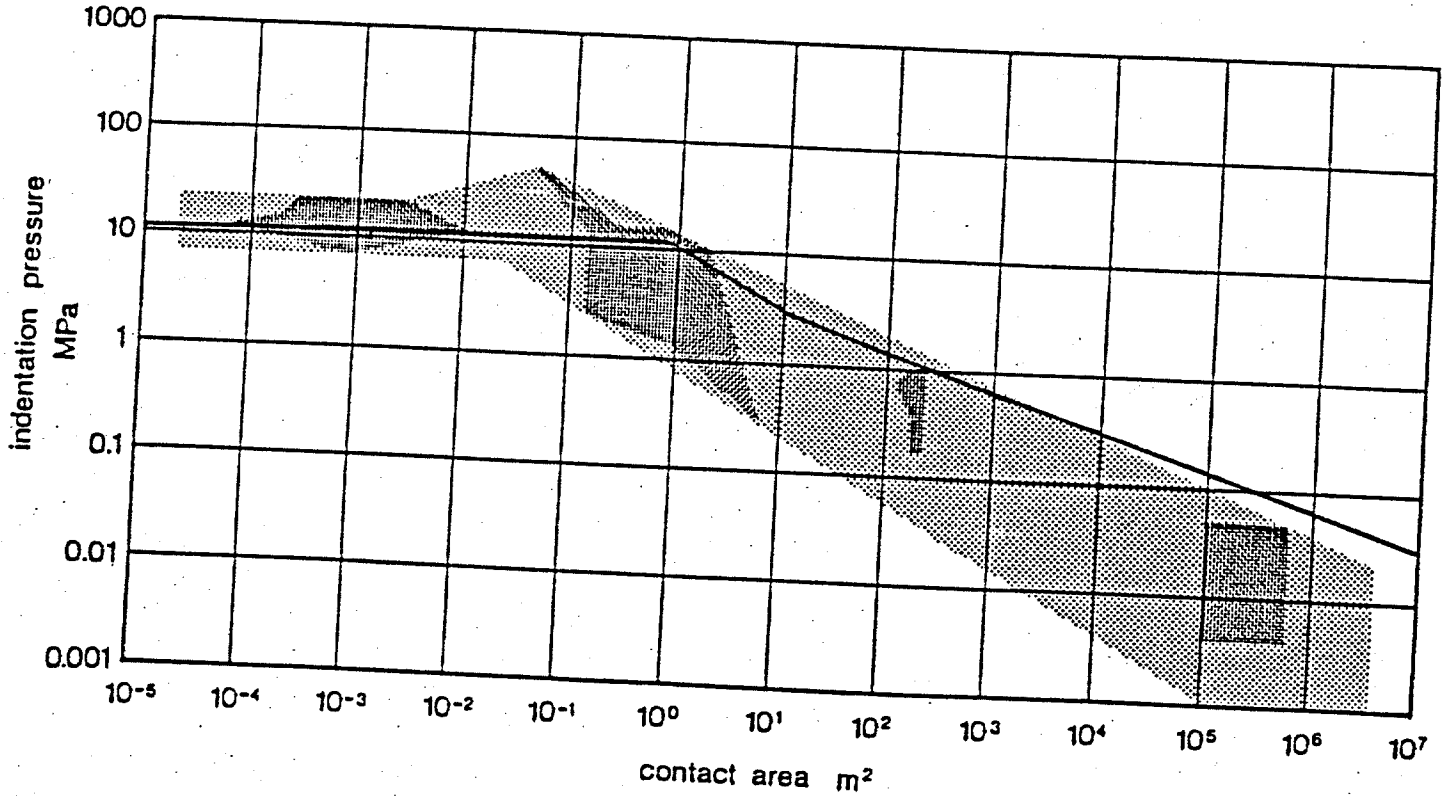

Fig. 6 - Pressure-Area Curve

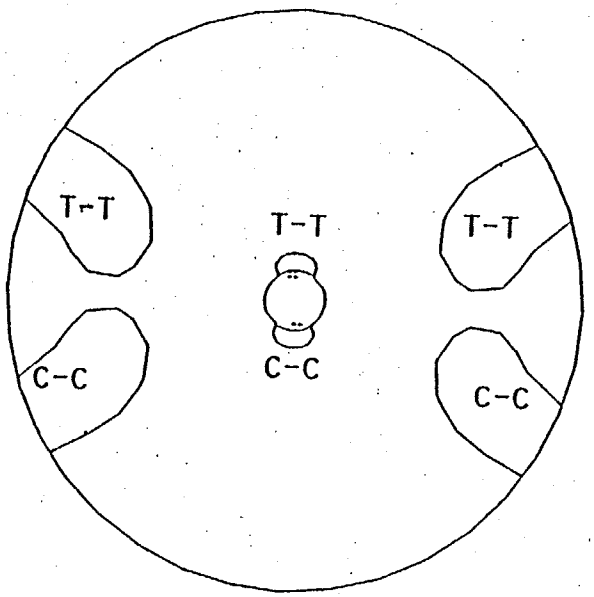

(a) Time Step 1

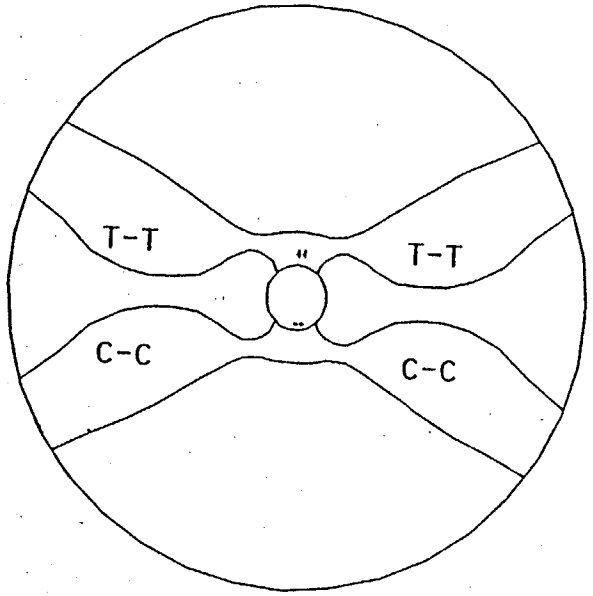

(b) Time Step 20

Fig. 7 - Biaxial Stress Regions for Fixed Condition

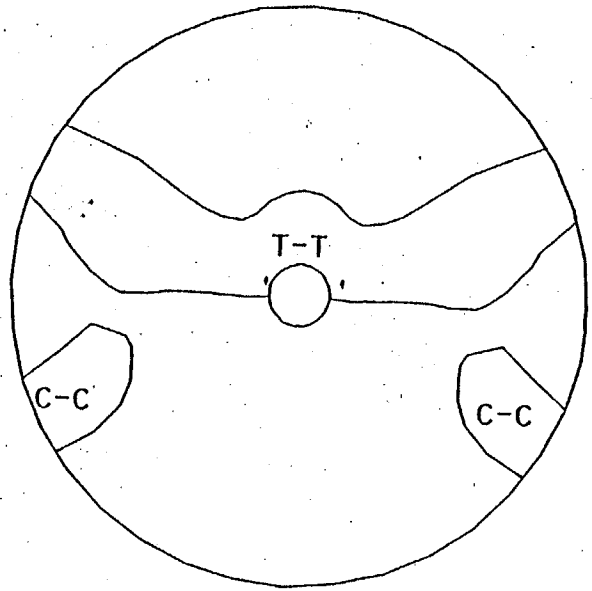

(a) Time Step 1

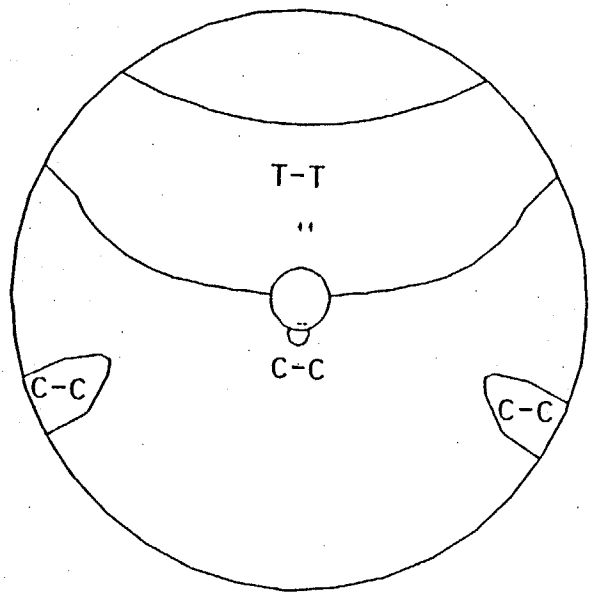

(b) Time Step 20

Fig. 8 - Biaxial Stress Regions for Free Condition

Maximum Principal Strain
Contour Levels
A = 0.0
B = 0.0005
C = 0.0010
D = 0.0015
E = 0.0020
F = 0.0025

Minimum Principal Strain
Contour Levels
A = -0.0030
B = -0.0025
C = -0.0020
D = -0.0015
E = -0.0010
F = -0.0005
G = 1.2×10^{-10}

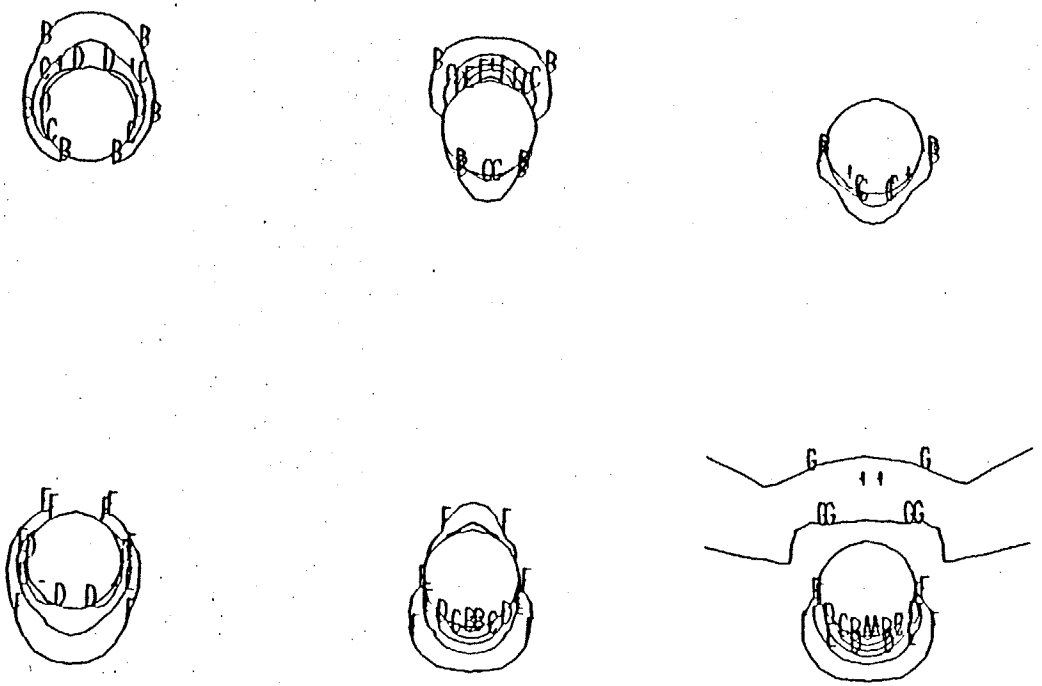

(a) Fixed (b) Roller (c) Free

Fig. 9 - Principal Strain Contours (Time Step 20)

Contour Levels

A = 0.5 x 10^{-6}

B = 1.5 x 10^{-6}

C = 2.5 x 10^{-6}

D = 3.5 x 10^{-6}

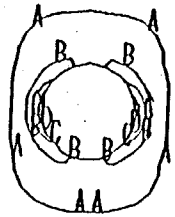

(a) Fixed

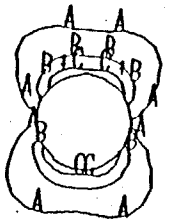

(b) Roller

(c) Free

Fig. 10 - Effective Strainrate Contours (Time Step 20)

S. Shyam Sunder and Seng-Kiong Ting
Department of Civil Engineering
Massachusetts Institute of Technology
Room 1-274, Cambridge, MA 02139 USA

DUCTILE TO BRITTLE TRANSITION IN SEA ICE UNDER UNIAXIAL LOADING

Abstract

A new constitutive model for sea ice, applicable to monotonic uniaxial loading in both compression and tension, is proposed. The stress-strain-strainrate behavior of sea ice is modelled accounting for strain softening and for fracture which manifests itself in terms of tensile cracking and crushing in compression. The model is used to predict first cracking in ice under uniaxial compressive loading based on a limiting tensile strain criterion and the results are calibrated with experimental data available in the literature.

1 INTRODUCTION

Field observations of sea ice indentation on offshore structures in the Arctic show that fracture processes are a major factor in ice-structure interaction.

The occurrence of first cracks in ice under compressive creep conditions in the laboratory has been studied by Gold /2/. Based on the assumption that grain boundary shear or sliding can be associated with a delayed elastic effect, Sinha /10/ postulated that

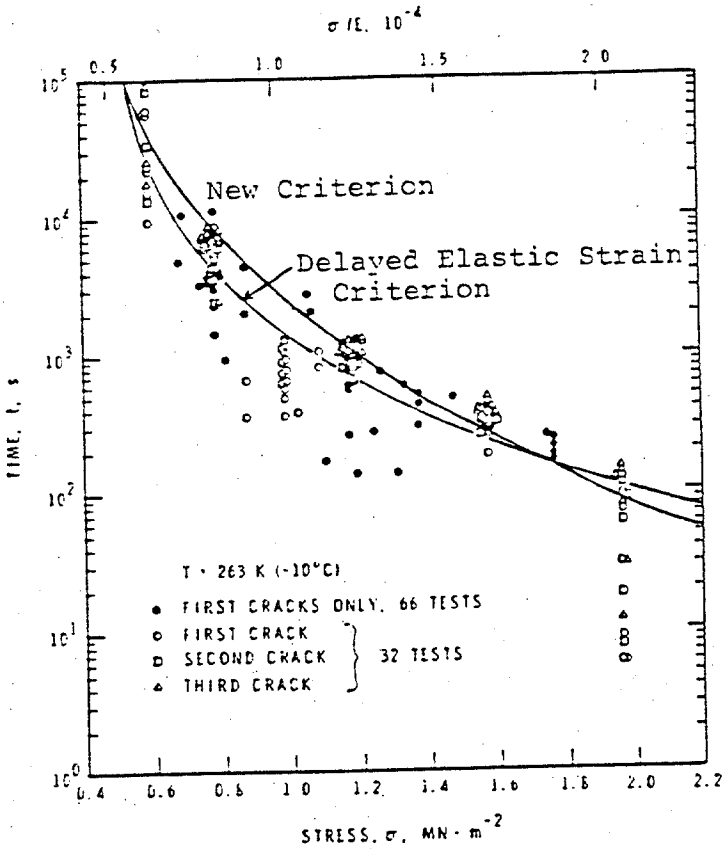

Fig. 1 Formation of first cracks during uniaxial compressive creep tests.

delayed elasticity can be linked to crack nucleation. With the help of his mathematical model for delayed elasticity and the experimental data of Gold, he showed that for S-2 ice of grain size 4.5 mm cracks begin to form if the delayed elastic strain exceeds 1.04×10^{-4}. The time to formation of first crack based on Gold's laboratory experiments and Sinha's delayed elastic strain criterion is plotted in Fig. 1.

A suddenly applied constant load case, i.e., creep, is not representative of loading conditions on offshore structures. A constant strainrate or stress-rate condition may be more realistic. Sanderson and Child /8/ consider typical stress-rates of 0.010-0.035 kPa s^{-1} and extreme stress-rates of 1-5 kPa s^{-1}. Using the principle of superposition, which Sinha /11/

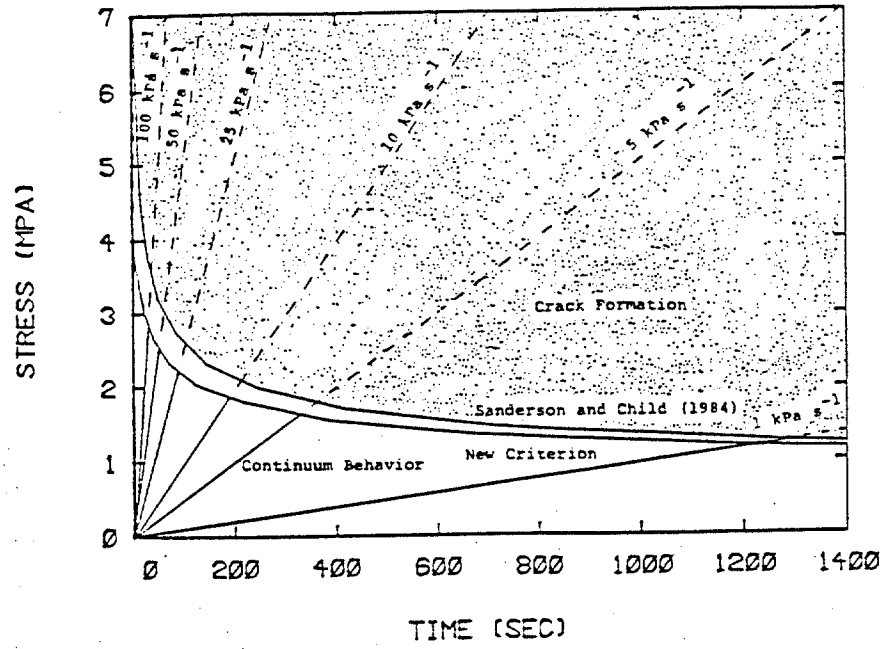

Fig. 2 Formation of first cracks during tests at constant stress-rate.

has shown to be valid for "icelike" materials under monotonically increasing stress, and the delayed elastic strain criterion they predict that first cracks in pure S-2 ice should typically occur at a stress of 0.6-0.7 MPa and in extreme conditions may occur at 1.3-1.8 MPa (Figs. 2 and 3). For sea ice, the stress levels are corrected by altering the net section stress due to brine volume as described by Sanderson /7/. The corresponding stresses are 0.4 MPa and 0.8-1.1 MPa (Fig. 4).

In order to explain the well-known discrepancy in ice forces between predictive models which use mechanical properties obtained in the laboratory and actual field measurements, Sanderson and Child /8/ propose that formation of first cracks in the field is synonymous with failure of the ice. As such, the stress levels identified in the previous paragraph are considered to limit ice forces. Although intuitively appealing, it is not clear how this failure criterion

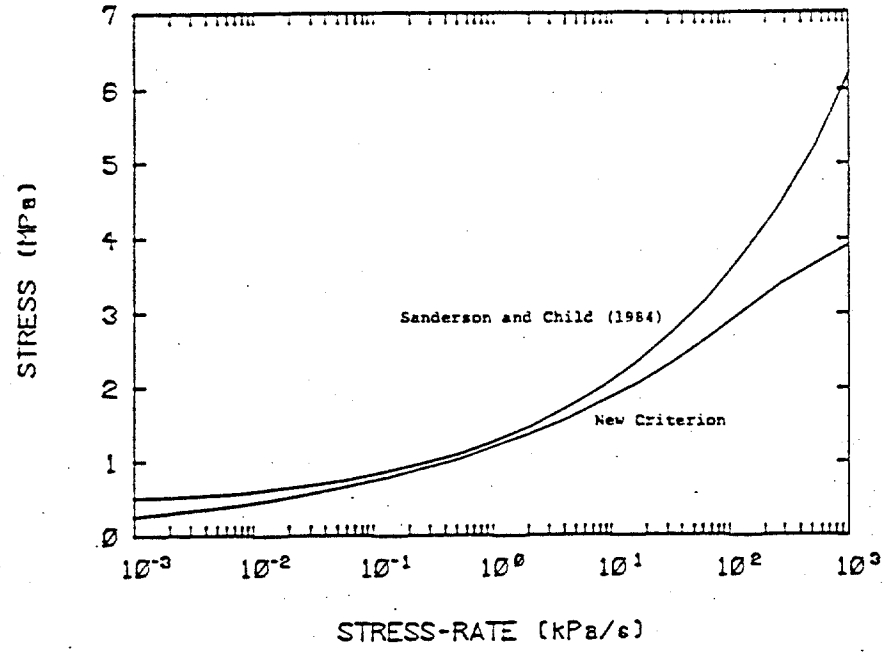

Fig. 3 Stress at which first cracks appear for pure ice at constant stress-rates.

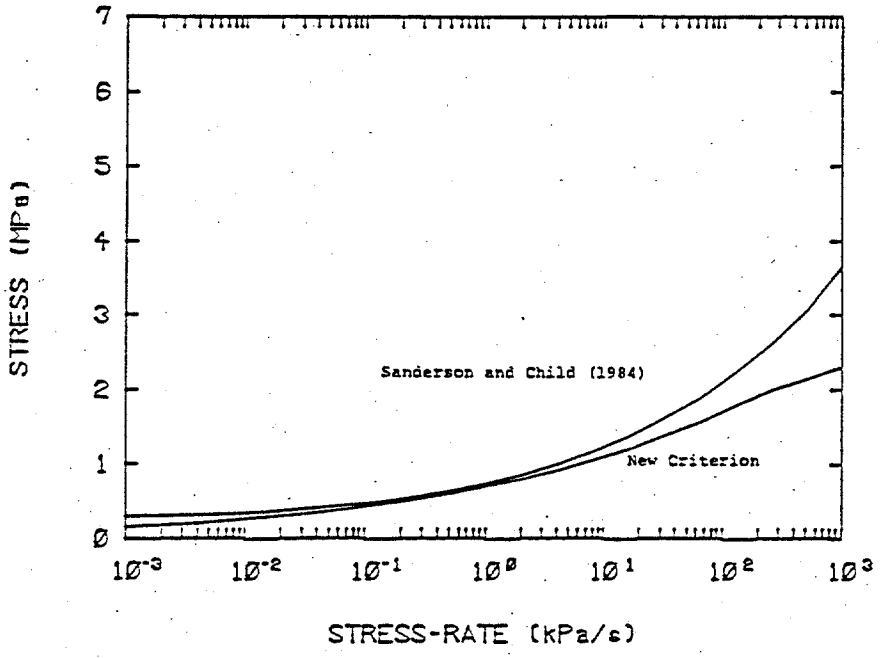

Fig. 4 Stress at which first cracks appear for sea ice at constant stress-rates.

can be incorporated in a finite element analysis framework for ice force prediction.

Fracture manifests itself in terms of tensile cracking and crushing in compression. Numerical analysis of ice-structure interaction processes in the creeping mode of deformation /1/ indicates that tensile stresses occupy a large fraction of the area of an ice sheet. Since ice is weaker in tension than in compression once cracks occur, accounting for the differing behavior of ice in tension may help to reduce ice force predictions significantly.

This paper presents a new constitutive model for sea ice, applicable to monotonic uniaxial loading in both compression and tension. The stress-strain-strainrate behavior of ice is modelled accounting for strain softening and fracture. The model is used to predict the occurrence of first cracks in ice under uniaxial compressive loading. Tensile strains occur under this loading condition as a result of the Poisson effect or incompressibility condition. Once cracks occur, the material continues to sustain compressive load but loses its ability to carry tensile loads in the transverse direction if applied. This is a realistic assumption and is often used in modeling concrete behavior /12/. A limiting tensile strain criterion dependent on the instantaneous strainrate in tension is developed to predict crack nucleation. The results for compressive creep compare very well with the experimental data of Gold /2/.

2 NEW UNIAXIAL CONSTITUTIVE MODEL

A phenomelogical approach based on simple thermo-rheological models has been used in developing the new

uniaxial constitutive model /13/. The model is based on Orowan's concept /5/ that material strength is affected simultaneously by work hardening or strain hardening and work softening or recovery. Fracture in pure ice is modelled using the 'strength'-strainrate data of Ashby and Cooksley contained in Palmer et al. /6/. The resulting model is consistent with Michel's /4/ schematic idealization of ice behavior.

For constant strainrates of up to 5×10^{-4} s^{-1} under compressive loading, the stress-strain-strainrate behavior of ice is given by:

$$\sigma = \frac{A}{M}\,\dot{\varepsilon}^{\frac{1}{N}}\,[1-\exp(-M\varepsilon)] - \frac{B}{L}\,\dot{\varepsilon}^{\frac{1}{K}-1}\,[1-\exp(-L\varepsilon)] \qquad (1)$$

where A=114025 MPa $s^{1/3}$, B=217408 MPa $s^{2/3}$, M=1411.2, L=430, N=3 and K=0.6 based on Wang's /14/ experimental data for sea ice. At strainrates greater than 10^{-2} s^{-1}, pure ice is assumed to fracture (crush) at a stress of 5.1 MPa and to behave as a linear elastic material with Young's modulus, E, equal to 9.5 GPa. The intermediate strainrates define the ductile-to-brittle transition in compression. For strainrates between 5×10^{-4} and 10^{-3} s^{-1}, the fracture strength is assumed to be 7.14 MPa and the stress-strain behavior up to fracture is given by Eq. (1). For strainrates in the range 10^{-3}-10^{-2} s^{-1}, a linear interpolation between 7.14 and 5.1 MPa on log-log scale is used to define the fracture strength, while the stress-strain behavior up to fracture is defined by Eq. (1) for a strainrate of 10^{-3} s^{-1} (the initial tangent modulus of Eq. (1) reaches a value of 9.5 GPa, the linear elastic modulus, at this strainrate).

Constant stress-rate and creep curves in compression generated with this model agree with Wang's

/14/ theoretical model and the experimental data used by him for calibration purposes. Moreover, the adopted modeling strategy avoids the numerical problems encountered by Wang.

The stress-strain-strainrate behavior in uniaxial tension prior to fracture is considered to be identical to that under uniaxial compression as given by Eq. (1). Hawkes and Mellor /3/ justify this assumption for creep data. For strainrates less than 3×10^{-8} s^{-1} (i.e., tension 'strength' of 0.42 MPa for pure ice and 0.25 MPa for sea ice), ice does not fracture in tension. For strainrates greater than 5×10^{-5} s^{-1}, tensile cracking occurs at a stress of 2.04 MPa. A linear interpolation on log-log scale is used for intermediate strainrates, defining the ductile-to-brittle transition in tension.

3 PREDICTION OF FIRST CRACK OCCURRENCE

The prediction of first crack occurrence under uniaxial compressive creep and constant stress-rate conditions is considered here. In order to make this prediction, it is necessary to monitor the tensile strains resulting from the Poisson effect or incompressibility condition and to compare them with the strain for tensile fracture at the instantaneous strainrate. When the actual instantaneous tensile strain becomes equal to the instantaneous fracture strain the first crack is assumed to occur. This is the limiting tensile strain criterion for crack nucleation. A numerical procedure is developed to make the crack prediction. A time increment not exceeding 10^{-5} divided by the instantaneous strainrate is necessary to obtain accurate results.

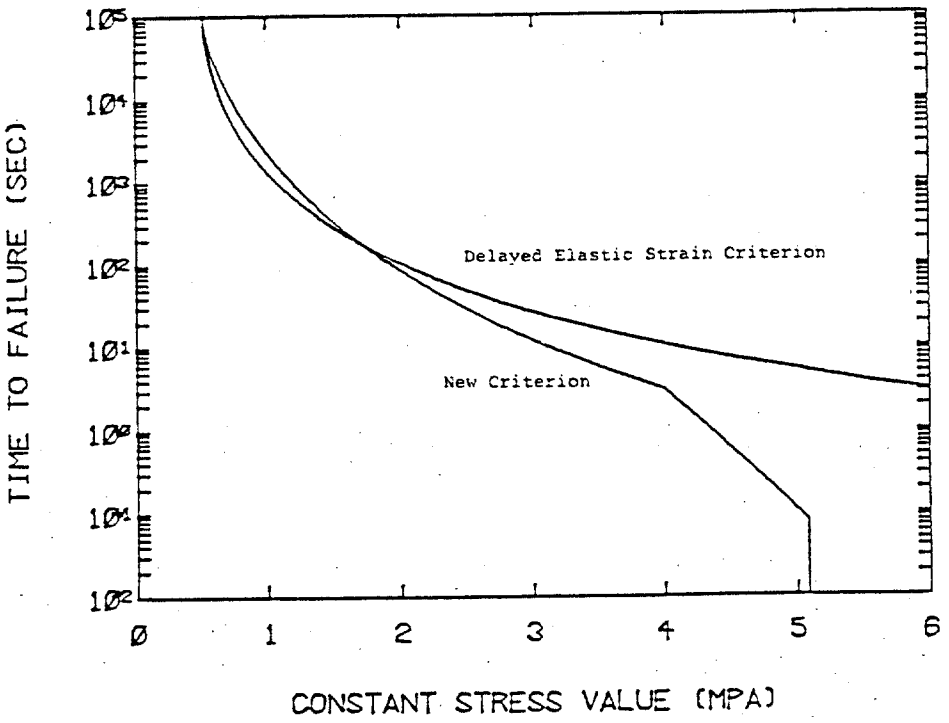

Fig. 5 Formation of first cracks in uniaxial creep up to the fracture stress in compression.

Figure 1 contains the prediction of first cracks using the limiting tensile strain criterion under creep conditions. Comparison with the experimental data of Gold shows that the proposed criterion is in excellent agreement with data. In particular, the time to first crack asymptotically approaches infinity as the compressive stress reduces to 0.52 MPa. The choice of stress-strainrate at which ice transits from ductile to fracture behavior in tension , i.e., 0.42 MPa and 3×10^{-8} s^{-1},defines this asymptote. The large scatter in the experimental results at σ=2 MPa is possibly due to the finite rise time of two seconds for the applied load to reach the constant stress state for ideal creep. The limiting tensile strain criterion compares well with the delayed elastic strain criterion of Sinha for the range of stresses considered in the figure. However, at higher stresses the two criteria are in significant disagreement (Fig. 5). At

the compressive fracture stress of 5.1 MPa, the proposed model predicts a zero time to first crack since no creep can occur under this loading. At stresses greater than about 4 MPa which corresponds to the leveling-off of the tensile fracture stress to 2.04 MPa, the tensile strain to fracture reduces faster than at lower stresses. This leads to a faster reduction in time to first crack. The sharp kink at the 4 MPa transition point can be eliminated by a smoother transition in the cracking criterion around the strainrate of 5×10^{-5} s^{-1}.

Figure 2 contains the prediction of first cracks under constant stress-rate conditions. The agreement between Sanderson and Child's analysis based on the delayed elastic strain criterion and the present criterion is very good in general. At infinite stress-rate, the stress at first crack is limited by the compressive fracture stress of 5.1 MPa. This is predicted by the proposed fracture criterion. Figures 3 and 4 show that for typical stress-rates the stress at first crack is 0.45-0.60 MPa for pure ice and 0.26-0.35 MPa for sea ice. For extreme stress-rates the corresponding numbers are 1.2-1.6 MPa and 0.7-0.9 MPa.

4 CONCLUSIONS

This paper has proposed a new uniaxial constitutive model for sea ice that accounts for strain softening and fracture (cracking and crushing). The adequacy of the model has been demonstrated by comparison with experimental data obtained under constant strainrate, creep, and constant stress-rate conditions. A limiting tensile strain criterion has been postulated to predict first cracks in ice and its

validity has been established by comparison with available experimental data.

The constitutive model is being extended to account for unloading and reloading conditions and for multiaxial stress states. The resulting model will be incorporated in a finite element analysis framework to predict indentation pressures and forces using the limiting tensile strain criterion for crack initiation and propagation. For load transmitting systems such as ice features (as opposed to load bearing structural systems) a limiting tensile strain criterion for fracture propagation is likely to be conservative when compared to a classical fracture mechanics approach. This is because the latter considers only the propagation of pre-existing cracks with a given distribution of sizes, while the former may be used to predict both the initiation and propagation of cracks in a material originally in virgin (flawless) form.

5 ACKNOWLEDGEMENTS

This research is funded by The Standard Oil Company (Ohio) through MIT's Center for Scientific Excellence in Offshore Engineering, and cosponsored by the U.S. Department of the Interior, Minerals Management Service.

6 REFERENCES

1. Chehayeb, F.S., Ting, S-K., Shyam Sunder, S. and Connor, J.J., Sea ice indentation in the creeping mode. Proc. of the 17th Annual Offshore Technology Conference, Paper OTC 5056, Houston, Texas, May 1985.

2. Gold, L.W., The process of failure of columnar-grained ice. Philosophical Magazine, Vol. 26, No. 2, 1972, pp. 310-328.

3. Hawkes, I. and Mellor, M., Deformation and

fracture of ice under uniaxial stress. Journal of Glaciology, Vol. 11, No. 61, 1972, pp. 103-131.

4. Michel, B., Advances in ice mechanics. The 6th int. conf. on Port and Ocean Engineering under Arctic Conditions (POAC). Quebec 1981. Universite Laval, Quebec 1981, pp.189-204.

5. Orowan, E. and Scott, J.W., The creep of metals. Journal of Iron and Steel Institute, Vol. 54, 1946, 45 p.

6. Palmer, A.C., Goodman, D.J., Ashby, M.F., Evans, A.G., Hutchinson, J.W., and Ponter, A.R.S., Fracture and its role in determining ice forces on offshore structures. Annals of Glaciology, Vol. 4, 1983, pp. 216-221.

7. Sanderson, T.J.O., Theoretical and measured ice forces on wide structures. Proc. 7th International Symposium on Ice, IAHR, Hamburg, August 1984, 32 p.

8. Sanderson, T.J.O. and Child, A.J., Ice loads on offshore structures: the transition from creep to fracture. 1984, 8 p.

9. Sinha, N.K., Rheology of columnar-grained ice. Experimental Mechanics, Vol. 18, No. 12, December 1978, pp. 464-470.

10. Sinha, N.K., Delayed elastic strain criterion for first cracks in ice. Proc. IUTAM Symposium on the Deformation and Failure of Granular Materials. Delft 1982, A.A. Balkema, Rotterdam, pp. 323-330.

11. Sinha, N.K., Creep model of ice for monotonically increasing stress. Cold Regions Science and Technology, Vol. 8, 1983, pp.25-33.

12. Task Committee on Finite Element Analysis of Reinforced Concrete Structures, Finite element analysis of reinforced concrete. ASCE, New York, NY 1982, 545 p.

13. Ting, S.K. and Shyam Sunder, S., Sea ice indentation accounting for strain-rate variation. Proc. of the ASCE Specialty Conference: Arctic '85 - Civil Engineering in the Arctic Offshore, San Francisco, California, March 1985, 11 p.

14. Wang, Y.S., A rate-dependent stress-strain relationship for sea ice. First International Symposium on Offshore Mechanics and Arctic Engineering, New Orleans, 1982, pp. 243-248.